The impact of snow nitrate photolysis on boundary layer chemistry and the recycling and redistribution of reactive nitrogen across Antarctica and Greenland in a global chemical transport model

Zatko, M.C.[1], Geng, L.[1], Alexander, B. [1], Sofen, E.D.[1,2], Klein, K.[3]

[1]Department of Atmospheric Sciences, University of Washington, Seattle, United States
[2]now at MathWorks, Natick, MA, United States
[3]Division of Glaciology, Alfred Wegener Institute Helmholtz Centre for Polar and Marine Research, Bremerhaven, Germany

Correspondence to Becky Alexander (beckya@uw.edu)

Abstract
The formation and recycling of reactive nitrogen (NO, NO_2, HONO) at the air-snow interface has implications for air quality and the oxidation capacity of the atmosphere in snow-covered regions. Nitrate (NO_3^-) photolysis in snow provides a source of oxidants (e.g., hydroxyl radical) and oxidant precursors (e.g., nitrogen oxides) to the overlying boundary layer, and alters the concentration and isotopic (e.g., $\delta^{15}N$) signature of NO_3^- preserved in ice cores. We have incorporated an idealized snowpack with a NO_3^- photolysis parameterization into a global chemical transport model (GEOS-Chem) to examine the implications of snow NO_3^- photolysis for boundary layer chemistry, the recycling and redistribution of reactive nitrogen, and the preservation of ice-core NO_3^- in ice cores across Antarctica and Greenland, where observations of these parameters over large spatial scales are difficult to obtain. A major goal of this study is to examine the influence of meteorological parameters and chemical, optical, and physical snow properties on the magnitudes and spatial patterns of snow-sourced NO_x fluxes and the recycling and redistribution of reactive nitrogen across Antarctica and Greenland. Snow-sourced NO_x fluxes are most influenced by temperature-dependent quantum yields of NO_3^- photolysis, photolabile NO_3^- concentrations in snow, and concentrations of light-absorbing impurities (LAI) in snow. Despite very different assumptions about snowpack properties, the range of model-calculated snow-sourced NO_x fluxes are similar in Greenland (0.5 to 11×10^8 molec cm^{-2} s^{-1}) and Antarctica (0.01 to 6.4×10^8 molec cm^{-2} s^{-1}) due to the opposing effects of higher concentrations of both photolabile NO_3^- and LAI in Greenland compared to Antarctica. Despite the similarity in snow-sourced NO_x fluxes, these fluxes lead to smaller factor increases in mean austral summer boundary layer mixing ratios of total nitrate ($HNO_3 + NO_3^-$), NO_x, OH, and O_3 in Greenland compared to Antarctica because of Greenland's proximity to pollution sources. The degree of nitrogen recycling in the snow is dependent on the relative magnitudes of snow-sourced NO_x fluxes versus primary NO_3^- deposition. Recycling of snow nitrate in Greenland is much less than in Antarctica because the deposition of primary NO_3^- is up to 35 times larger than snow-sourced NO_x fluxes in Greenland. Photolysis-driven loss of snow NO_3^- is largely dependent on the time that NO_3^- remains in the snow photic zone (up to 6.5 years in Antarctica and 7 months in Greenland), and wind patterns that redistribute snow-sourced reactive nitrogen across Antarctica and Greenland. The loss of snow NO_3^- is higher in Antarctica (up to 99%) than in Greenland (up to 83%) due to deeper snow photic zones and lower snow accumulation rates in Antarctica. Modeled enrichments in ice-core $\delta^{15}N(NO_3^-)$ due to photolysis-driven loss of snow NO_3^- ranges from 0 to 363‰ in Antarctica and 0 to 90‰ in Greenland, with the highest fraction of NO_3^- loss and largest enrichments in ice-core $\delta^{15}N(NO_3^-)$ at high elevations where snow accumulation rates are lowest. There is a strong relationship between the degree of photolysis-driven loss of snow NO_3^- and the degree of nitrogen recycling between the air and snow throughout all of Greenland and in Antarctica where snow accumulation rates are greater than 130 kg m^{-2} a^{-1} in the present day.

1. Introduction

Nitrogen oxides (NO_x=NO+NO_2) emitted from fossil fuel combustion, biomass burning, soil microbial activity, and lightning have adverse respiratory effects, contribute to the formation of atmospheric acidity, and are a key ingredient in tropospheric oxidant cycling leading to the formation of ground-level ozone (O_3). O_3 also has adverse respiratory effects, is an effective greenhouse gas [*UNEP*, 2011], and its photolysis dominates hydroxyl radical (OH) production in much of the troposphere [*Thompson*, 1992]. Oxidation to form nitrate (HNO_3/NO_3^-) is the main sink for NO_x in the troposphere [*Logan*, 1983], and the lifetime of NO_x against oxidation to nitrate is expected to be 1-3 days in polar regions [*Levy et al*., 1999]. NO_3^- is lost from the atmosphere through dry and wet deposition to the Earth's surface, and has a global atmospheric lifetime of roughly 5 days [*Xu and Penner*, 2012]. In Antarctica and Greenland, HNO_3 and NO_3^- deposited to the snowpack originates from both the troposphere (e.g., long-range transport) [*Geng et al*., 2014a, *Lee et al*., 2014, *Wespes et al*., 2012] and stratosphere [*Davidson et al*., 1989, *Frey et al*., 2009, *Savarino et al*., 2007]. In snow-covered regions, the deposition of HNO_3 and NO_3^- is not a permanent sink for NO_x, as the photolysis of snow NO_3^- returns reactive nitrogen (N_r=NO_x, HONO) back to the atmosphere, with implications for other oxidants such as OH and O_3 [*Domine and Shepson,* 2002].

Snow photochemistry significantly influences boundary layer chemistry and plays an important role in oxidant production and cycling, especially in pristine regions, such as Antarctica [*Bloss et al*., 2007, *Chen et al*., 2004, 2007,*Grannas et al*., 2007, *Helmig et al*., 2008,*Sjostedt et al*., 2007, *Thomas et al*., 2012]. Snow photochemistry may have more widespread impacts since up to 40% of land on Earth is snow-covered at a given time [*Grannas et al*., 2007]. NO_3^- is not the only photochemically-active species in snow. The photolysis of nitrite (NO_2^-) in snow and the photolysis of snow-sourced formaldehyde (CH_2O), nitrous acid (HONO), and hydrogen peroxide (H_2O_2) provide additional sources of N_r and OH to the boundary layer. Bromine (Br_2) is also produced in the snow via reactions involving bromide (Br^-), photochemically-active species (e.g., NO_3^-), and photochemically-produced species (e.g., OH) within snow grains [*Pratt et al*., 2013].

In snow, NO_3^- photolysis likely occurs in the liquid-like region (LLR) on the surface of ice grains, in cracks between ice grains, or in brine pockets embedded within ice grains [*Domine et al*., 2013]. There are two channels for NO_3^- photolysis at wavelengths (λ)=290-345 nm. In the aqueous phase, NO_3^- can photolyze to produce NO_2 and OH (E1), or produce NO_2^- and $O(^3P)$ (E2), but E1 is thought to be the dominant pathway [*Grannas et al*., 2007, *Mack and Bolton*, 1999, *Meusinger et al*., 2014].

$$NO_3^-(aq) + h\nu(+H^+) \rightarrow NO_2(aq) + OH(aq), \quad \text{E1}$$

$$NO_3^-(aq) + h\nu \rightarrow NO_2^-(aq) + O(^3P)(aq), \quad \text{E2}$$

The aqueous phase NO_2 produced in E1 can evaporate to the gas phase and be released into the interstitial air [*Boxe et al.,* 2005] and subsequently be transported to the overlying atmosphere via diffusion and windpumping [*Zatko et al*., 2013]. The quantum yield (ϕ) in E1 is strongly influenced by the location of NO_3^- in an ice grain. Quantum yields are

more weakly dependent on LLR temperature and pH; ϕ values increase with increasing temperature and pH [*Chu and Anastasio*, 2003]. Chu and Anastasio [2003] froze NO_3^--doped water in the lab and measured the quantum yield for E1 (0.003 molec photon^{-1} at T=253 K) as frozen ice grains were exposed to ultraviolet (UV) radiation. Zhu et al. [2010] deposited HNO_3 on an ice film and measured ϕ for E1 (0.6 molec photon^{-1} at T=253 K), as the frozen surface was irradiated with UV radiation. A recent study by Meusinger et al. [2014] found ϕ=0.003-0.44 molec photon^{-1} at T=258 K for E1, which nearly spans the full range of previously reported quantum yields. Results from Meusinger et al. [2014] suggest that ϕ is dependent on the length of time that snow is exposed to UV radiation, as well as the location of NO_3^- in the ice grain. Meusinger et al. [2014] suggest that two photochemical domains of NO_3^- exist: photolabile NO_3^- and NO_3^- buried within the ice grain. The NO_x produced from the photolysis of photolabile NO_3^- can escape the ice grain, while the NO_x produced from the photolysis of buried NO_3^- is likely to undergo recombination chemistry within the snow grain, thus lowering the quantum yield of NO_x for NO_3^- photolysis. Recombination chemistry involves NO_3^- reformation from photo-products (e.g., NO_x and OH) within the ice grain, which alters oxygen isotopes (e.g., $\Delta^{17}O$) of NO_3^-, but does not impact bulk snow NO_3^- concentrations nor its nitrogen isotopes ($\delta^{15}N$) [*Frey et al*., 2009, *Erbland et al*., 2013, 2015].

The NO_2^- produced in E2 is quickly photolyzed at longer wavelengths (λ=290-390 nm) in the LLR or can react with OH or H^+ in the LLR to produce N_r [*Grannas et al*., 2007]:

$$NO_2^-(aq) + h\nu(+H^+, aq) \rightarrow NO(aq) + OH(aq), \quad \text{E3}$$
$$NO_2^-(aq) + OH(aq) \rightarrow NO_2(aq) + OH^-(aq), \quad \text{E4}$$
$$NO_2^-(aq) + H^+(aq) \rightarrow HONO(aq), \quad \text{E5}$$

HONO produced in E5 can rapidly photolyze to produce NO and OH in the interstitial air or the atmospheric boundary layer [*Anastasio and Chu*, 2009]. Reactions involving NO_2^- are intermediate reactions for NO_3^- photolysis because NO_3^- photolysis is required for NO_2^- formation and the end products of E1-E5 are all N_r. Once produced, NO_2 and NO can be efficiently transported to the overlying atmosphere via windpumping [*Zatko et al*., 2013] and enter into rapid NO_x-cycling reactions. In the atmosphere, the relative abundance of NO and NO_2 will be determined by local atmospheric conditions, specifically oxidant concentrations (e.g., O_3, HO_2, RO_2, BrO, and ClO) [*Frey et al.,* 2013]. The snow-sourced NO_x can be re-oxidized to HNO_3 via E6 under sunlit conditions.

$$NO_2(g) + OH(g) \rightarrow HNO_3(g), \quad \text{E6}$$

The HNO_3 produced in E6 can undergo wet or dry deposition to the snow surface [*Dibb et al*., 2004] within a day [*Slusher et al*., 2002, *Wang et al*., 2008]. Evidence for HNO_3 re-deposition is seen in the snow NO_3^- concentration profile at many polar locations, where NO_3^- concentrations may be over an order of magnitude higher in the top two centimeters (cm) of snow compared to NO_3^- concentrations below [*Dibb et al*., 2004, *Frey et al*., 2009, *Mayewski and Legrand*, 1990, *Rothlisberger et al*., 2000].

Once HNO_3 is deposited back to the snow, it is available for photolysis again. NO_3^- can be recycled multiple times between the boundary layer and the snow before burial below the photochemically-active region, known as the snow photic zone [*Davis et al*., 2008, *Erbland et al*., 2015]. Only two previous studies have attempted to quantify the degree of nitrogen recycling between the air and snow. Davis et al. [2008] use estimates of atmospheric NO_x overhead-column burdens and average atmospheric NO_x lifetimes along with primary nitrogen deposition measurements from Legrand and Kirchner [1990] to estimate that nitrogen is recycled 1.8 times on average between the air and snow in one photochemical season in East Antarctica, although this value may be 3 to 5 times higher due to uncertainties in primary nitrogen deposition estimates. Erbland et al. [2015] use a multi-layer, one-dimensional snow model (TRANSITS) and calculate that nitrogen is recycled 4 times on average before burial beneath the snow-photic zone. Erbland et al. [2015] observe an inverse relationship between snow accumulation rate and nitrogen recycling in regions where snow accumulation rates are greater than 50 kg m^{-2} a^{-1}, and suggest that in these regions, the degree of NO_3^- recycling is governed by the time NO_3^- remains in the snow photic zone.

The photolysis of snow NO_3^- and subsequent recycling between the air and snow alters the concentration and isotopic (e.g., $\delta^{15}N$) signature of NO_3^- that is ultimately preserved in polar ice sheets, which hampers the interpretation of ice-core NO_3^- records [*Wolff et al*., 2008]. Such records have been sought to reconstruct the past history of the abundance of NO_x in the atmosphere [*Wolff*, 1995]. It has also been suggested that the nitrogen ($\delta^{15}N$) and oxygen ($\Delta^{17}O$) isotopic composition of ice-core NO_3^- can provide information on past variability in atmospheric NO_x sources and oxidant abundances [e.g., *Alexander et al*., 2004, *Hastings et al*., 2005]. Different sources of NO_x have different $\delta^{15}N$ signatures (~ -19‰ to 25‰, [*Geng et al*., 2014a, *Walters et al*., 2015]), giving ice-core $\delta^{15}N(NO_3^-)$ measurements the potential to track NO_x-source changes over time.

Ice-core $\delta^{15}N(NO_3^-)$ values will be altered if there is photolysis-driven loss of NO_3^- from the snow when snow-sourced NO_x is transported away from the site of primary deposition. Nitrate photolysis in snow is associated with a large fractionation constant (ε, e.g., -47.9‰ [Berhanu et al., 2014]), providing the boundary layer with a source of NO_x that is highly depleted in $\delta^{15}N(NO_3^-)$, leaving highly enriched $\delta^{15}N(NO_3^-)$ in the snow. In Antarctica, atmospheric $\delta^{15}N(NO_3^-)$ values at the coast are as low as -40‰, indicating transport of snow-sourced NO_x from the continental interior [*Morin et al*., 2009], while on the East Antarctica plateau, snow $\delta^{15}N(NO_3^-)$ up to 480‰ has been reported [*Blunier et al*., 2005, *Erbland et al*., 2013, *Frey et al*., 2009, *Shi et al.,* 2014], indicating net loss of NO_3^- driven by photolysis. In Greenland, atmospheric $\delta^{15}N(NO_3^-)$ values are much less depleted (as low as -15‰) and snow $\delta^{15}N(NO_3^-)$ values are much less enriched (as high as 15‰) compared to these extreme values observed in coastal Antarctica and on the East Antarctic plateau [*Geng et al*., 2014a, *Hastings et al*., 2004, *Jarvis et al*., 2009].

If snow-sourced NO_x is simply re-deposited back to the snow surface at the site of emission, a vertical profile in $\delta^{15}N(NO_3^-)$ within the snow photic zone will develop due to vertical redistribution of NO_3^- [*Erbland et al*., 2013, *Frey et al*., 2009]; however, the depth-integrated $\delta^{15}N(NO_3^-)$ will not be impacted, even with active photolysis-driven

recycling between the atmosphere and the snow. Enrichment in ice-core $\delta^{15}N(NO_3^-)$ requires photolysis-driven loss from snow from net atmospheric transport of snow-sourced NO_x away from the locations of its production. In addition to photolysis, ice-core $\delta^{15}N(NO_3^-)$ values are also influenced by evaporation of HNO_3 [*Mulvaney et al*., 1998] from snow and by atmospheric processing, such as NO_x cycling [*Freyer et al*., 1993] and gas-particle partitioning [*Heaton et al*., 1997, *Geng et al*., 2014a]; however, these impose a fractionation in $\delta^{15}N(NO_3^-)$ at least an order of magnitude smaller than photolysis, and are thus not able to explain the large enrichments in snow $\delta^{15}N(NO_3^-)$ observed on the East Antarctic plateau [*Blunier et al*., 2005, *Erbland et al*., 2013, *Frey et al*., 2009, *Shi et al.,* 2014].

Here we incorporate an idealized snowpack with a NO_3^- photolysis parameterization into a global chemical transport model. The idealized Antarctic and Greenland ice sheets in the model have similar properties as the real ice sheets, but are subject to assumptions about the chemical and physical properties of the snow. The idealized snowpacks in this modeling framework attempt to account for the spatial variability in parameters important to snow NO_3^- photolysis in order to investigate the potential spatial variability in snow-sourced NO_x fluxes, reactive nitrogen recycling and redistribution, and preservation of ice-core NO_3^- across Antarctica and Greenland, where observations of these parameters over large spatial scales are difficult to obtain. A major advantage of using a global chemical transport model framework is the ability to examine the potential redistribution and loss of reactive nitrogen due to photolysis-driven loss of snow NO_3^- across large spatial scales. The sensitivity of many parameters, such as snow accumulation rate, on the flux of snow-sourced NO_x, nitrogen recycling, and loss of snow NO_3^- is elucidated by comparing modeled results in Antarctica and Greenland. Section 2 describes the inclusion of an idealized snowpack with a snow NO_3^- photolysis parameterization into a global chemical transport model, GEOS-Chem. Section 3 explores the implications of photolysis-driven reactive nitrogen recycling and redistribution for boundary layer chemistry and the alteration of NO_3^- concentration and its nitrogen isotopes ($\delta^{15}N$) ultimately archived in ice cores. In section 3, we also compare model results in Antarctica and Greenland to examine the sensitivity of the flux of snow-sourced NO_x and associated photolysis-driven processes on meteorological parameters and various chemical, optical, and physical properties of snow. We end section 3 by discussing results from our model sensitivity studies that highlight the largest uncertainties in our ability to model these processes. Section 4 summarizes our conclusions and provides recommendations for future laboratory and field studies based on our model sensitivity results.

2. Methods

2.1. Incorporating Snow NO_3^- Photolysis into a Global Chemical Transport Model

Table 1 provides a glossary of the variables used throughout this paper.

2.1.1. Global Chemical Transport Model Description

GEOS-Chem is a global 3-dimensional (3-D) model of coupled aerosol-oxidant chemistry with detailed HO_x-NO_x-VOC-O_3-BrO_x tropospheric chemistry originally described in Bey et al. [2001]. The model uses assimilated meteorological data from the

NASA Goddard Earth Observing System (GEOS-5) including winds, convective mass fluxes, boundary layer depths, temperature, precipitation, and surface properties. Meteorological data have 6-hour temporal resolution (3-hour for surface variables and mixing depths). The TPCORE advection algorithm [*Lin and Rood*, 1996] is the transport routine in GEOS-Chem and is based on the calculation of the slopes between neighboring grid boxes. At the poles, neighboring grid boxes are used to estimate transport of chemical species into and out of the circular polar grid box. In Figures 2-11, data in each grid box are smoothed using bilinear interpolation. The spectral direct and diffuse downwelling surface irradiance and photolysis frequencies are calculated using the Fast-JX radiative transfer module [*Bian and Prather*, 2002, *Mao et al*., 2010, *Wild et al*., 2000]. In GEOS-Chem, aerosols can be wet deposited via scavenging in convective updrafts and by rainout from convective anvils and large-scale precipitation [*Liu et al*., 2001]. The wet deposition scheme for gases is described by Amos et al. [2012] and the scavenging of aerosol by snow and cold/mixed precipitation is described by Wang et al. [2011]. Dry-deposition velocities for coarse mode aerosols (radii between 1-10 mm) are calculated based on aerosol size and hydroscopic growth as described in Zhang et al. [2001]. Aerosol deposition to snow and ice surfaces is described by Fisher et al. [2011]. For smaller aerosols (radii less than 1 μm), dry deposition velocities are calculated with a standard resistance-in-series scheme [*Wang et al*., 1998, *Wesely*, 1989].

Anthropogenic NO_x emissions are from the EDGAR 3.2-FT2000 global inventory for the year 2000 [*Oliver et al*., 2005], scaled by country on the basis of energy statistics as described by van Donkelaar et al. [2008]. The monthly inventory of emissions from biomass burning are from the Global Fire Emissions Database (GFED2) [*van der Werf et al.,* 2009]. Soil NO_x emissions are computed using a parameterization described in Hudman et al. [2012], which is a function of vegetation type, temperature, soil moisture, precipitation, and fertilizer emissions. Emissions of NO_x from lightning are linked to deep convection following the parameterization of *Price and Rind* [1992] and are scaled globally as described by Murray et al. [2012] to match OTD/LIS climatological observations of lightning flashes. The stratospheric source of NO_y ($=NO_x+HNO_3$) utilizes monthly climatological 3-D production and loss rates from the Global Modeling Initiative (GMI) model [*Allen et al*., 2010], which captures the formation of the polar vortex and PSC sedimentation [*Murray et al*., 2012].

For this work, GEOS-Chem version v9-01-01 was run at 2°x2.5° horizontal resolution with 72 hybrid vertical levels using GEOS-5 meteorology from May 2009 to May 2010. The model was spun up for six months prior to May 2009. There are no sub-surface (snow) layers in GEOS-Chem and the three lowest vertical levels are each roughly 100 meters in height above Antarctica. The boundary layer in GEOS-Chem is calculated using a parameterization involving the bulk Richardson number with surface friction, a turbulent velocity scale, and non-local fluxes of heat and moisture [*Holtslag and Boville*, 1993] as implemented by Lin and McElroy [2010]. The mixing of emissions, dry deposition, and concentrations of individual species within the boundary layer are determined by static instability. In a stable boundary layer, the local scheme based on eddy diffusivity-theory is used, and the mixing is weak. In an unstable boundary layer, boundary layer mixing is triggered by large eddies. Average boundary layer mixing ratios

(ppbv) of species reported in this study (e.g., NO_3^-, NO_x, OH, O_3) are mixing ratios in the lowest vertical grid box (total height ~ 100 m).

Figure 1 illustrates the nitrogen recycling associated with snow NO_3^- photolysis as included in the model. The total flux of snow-sourced NO_x from the snow, F_{NOx} (molec cm^{-2} s^{-1}), is calculated using the wavelength-dependent absorption cross-section for NO_3^- photolysis (σ_{NO3^-}, cm^2 $molec^{-1}$), the temperature (T)- and pH-dependent quantum yield for NO_3^- photolysis (ϕ, molec $photon^{-1}$), the depth- and wavelength-dependent actinic flux in the snow photic zone (I, photons cm^{-2} s^{-1} nm^{-1}), and the average NO_3^- concentration ($[NO_3^-]$, molec cm^{-3}) integrated over the depth of the photic zone. F_{NOx} (molec cm^{-2} s^{-1}), is calculated in E7 and converted into units of ng N m^{-2} yr^{-1} in E9 and E10.

$$F_{NOx} = \int_{\lambda_0}^{\lambda_1} \int_{z_0}^{z_{3e}} J(\lambda, z) \cdot [NO_3^-]\, d\lambda dz\,, \qquad \text{E7}$$

where $[NO_3^-]$ is the average photolabile NO_3^- concentration over the depth of the snow photic zone ($z=z_0$ to $z= z_{3e}$) and J is the photolysis rate constant (s^{-1}), which is calculated in E8:

$$J = \sigma_{NO_3^-}(\lambda) \cdot \phi(T, pH) \cdot I(\lambda, z) \qquad \text{E8}$$

In E8, σ_{NO3^-} is from Sander et al. [2006]. The temperature-dependent ϕ from Chu and Anastasio [2003] (assumed constant pH of 5) is calculated using the modeled air temperature in the lowest vertical grid box. The actinic flux (I) is calculated at 1-cm intervals and integrated from the snow surface (z_0) to the depth of the photic zone (z_{3e}). The snow photic zone is defined as three times the e-folding depth of ultraviolet (UV) actinic flux in snow (z_{3e}), where 1 e-folding depth is z_e. Below z_{3e}, more than 95% of the radiation has been attenuated and minimal photochemistry occurs. The flux of snow-sourced NO_x is integrated over several ultraviolet wavelength bands (298-307 nm, 307-312 nm, 312-320 nm, 320-345 nm), which are then summed to calculate total F_{NOx} from the photolysis of snow NO_3^- between λ=298-345 nm. We assume that all NO_x formed in E7 is immediately evaporated and transported into the overlying boundary layer via wind pumping and diffusion [*Zatko et al.*, 2013].

2.1.2 Calculating Radiative Transfer in Snow

A 2-stream, plane parallel snowpack actinic flux parameterization based on a 4-stream radiative transfer model [*Grenfell*, 1991] was developed and described in detail in Zatko et al. [2013] and has been implemented into GEOS-Chem for the purposes of this study. The parameterization is simple, broadly applicable, and allows for variation in snow and sky properties (e.g., solar zenith angle, cloud fraction) over time. Ice grains are assumed to be spherical in shape and light-absorbing impurities (LAI), including black carbon, brown carbon, dust, and organics, are assumed to be homogeneously distributed throughout the snow and always external to the ice grain. The snowpack actinic flux parameterization is used to calculate the UV actinic flux (photons cm^{-2} s^{-1} nm^{-1}) and the mean summer e-folding depths (cm) across Antarctica and Greenland,, which are used to calculate F_{NOx}. The snowpack actinic flux parameterization is most sensitive to radiation equivalent mean ice grain radii (r_e) and insoluble LAI in snow [*Zatko et al.*, 2013]; higher

concentrations of LAI in the snow and smaller r_e lead to shallower e-folding depths (z_e). Vertical r_e and snow density (ρ_{snow}) profiles at Dome C, Antarctica from Gallet et al. [2011] are used across Antarctica for all seasons, which range from 86 to 235 μm and 260 to 360 kg m^{-3}, from the snow surface to 300-cm depth, respectively. Vertical r_e and ρ_{snow} profiles at Summit, Greenland from Carmagnola et al. [2013] are used in Greenland, ranging from 73 to 211 μm and 235 to 350 kg m^{-3}, from the snow surface to 300-cm depth, respectively.

The concentration of black carbon (BC) concentrations in snow (C_{BC}) are calculated using modeled total annual black carbon (hydrophilic + hydrophobic) deposition (ng BC m^{-2} yr^{-1}) and total annual snow accumulation rates (g H_2O m^{-2} yr^{-1}) in GEOS-Chem. At some locations in coastal Antarctica, high accumulation rates (up to 700 kg m^{-2} yr^{-1}) lead to unrealistically low C_{BC} (as low as 0.01 ng g^{-1}), therefore the minimum C_{BC} value used in the model is 0.08 ng g^{-1}, which is comparable to the C_{BC} values measured in high snow accumulation rate regions, such as in the East Antarctic sea ice zone (0.1 ng g^{-1}) [*Zatko and Warren*, 2015]. Insoluble non-black carbon species (nonBC) including dust, brown carbon, and organics, are responsible for the majority (up to 89% at λ=305 nm) of the absorption of radiation at UV wavelengths [*Zatko et al*., 2013] in snow. These nonBC species and their concentrations have not been well quantified in snow. Based on observations reported in Zatko et al. [2013], we scale UV-absorption by insoluble nonBC to the absorption by insoluble black carbon in snow by assuming that at λ=650-700 nm, which is a wavelength range where black carbon dominates absorption, insoluble black carbon is responsible for 70% of the particulate absorption. We also assume that nonBC material has an absorption Ångstrom exponent of 5 [*Doherty et al*., 2010].

We neglect the influence of soluble LAI in the snow and only consider the influence of insoluble LAI for calculations of actinic flux profiles in snow. To determine whether soluble LAI contribute significantly to light-absorption in the snow, we calculate the total extinction coefficient for insoluble BC, insoluble nonBC, and soluble LAI following section 2.1 of Zatko et al. [2013] and using the absorption coefficients for soluble material in snow reported in Beine et al., [2011] in northern Alaska. To our knowledge, observations of soluble light-absorbing impurities in Antarctic and Greenland snow are unavailable. We use soluble LAI observations from Alaska to provide a relative estimate of the importance of soluble LAI in polar snow. The absorption coefficients (0.028 m^{-1} at λ=307 nm) from Beine et al. [2011] are identical to the extinction coefficients because it is assumed that there is no scattering by soluble species. Insoluble C_{BC} (9 ng g^{-1}) from Barrow, Alaska [*Doherty et al*., 2010] were used to calculate extinction coefficients for insoluble BC and nonBC material and therefore the amount of nonBC absorption in the UV and near-visible wavelengths following Zatko et al. [2013]. Insoluble nonBC material is responsible for 9-14 times more absorption than soluble material in the wavelength range λ=298-345 nm. Insoluble BC material is responsible for 1.5-10 times more absorption than soluble material in the wavelength range λ=298-345 nm. The extinction coefficient is not influenced by the addition of a soluble absorber because scattering by snow grains dominates the extinction in snow. The effective co-albedo of single scattering is increased by 6-15% when soluble absorbers are included. The resulting change in z_e is at most 0.5 cm, which represents an increase of 4-9% in the

wavelength region of λ=298-345 nm.

2.1.3. Calculating NO_3^- Concentrations in Snow

The median value of sub-surface snow NO_3^- concentrations is 60 ng g^{-1} in Antarctica [*Bertler et al*., 2005] and 132 ng g^{-1} in Greenland [*Burkhart et al*., 2009]. Snow NO_3^- was collected over depths corresponding to between 1 and 70 year(s) of snow accumulation in Antarctica and between 1 and 148 year(s) of snow accumulation in Greenland. The observed median values of sub-surface snow NO_3^- concentrations are used for modeled sub-surface (from 2-cm depth to the bottom of the snow photic zone, z_{3e}) snow NO_3^- concentrations ($[NO_3^-]_{bot}$) across Antarctica and Greenland. Although there is a large variation in observed snow NO_3^- concentrations from the ITASE campaign [*Bertler et al*., 2005], there is no clear spatial pattern across Antarctica. In Greenland, the relationship between snow accumulation rate and snow NO_3^- concentrations is non-linear and snow accumulation alone cannot account for the spatial variability in NO_3^- concentrations in lower snow accumulation rate regions [*Burkhart et al*., 2009]. In Antarctica, snow NO_3^- concentrations in the top 2 cm of snow are up to 10 times higher than NO_3^- concentrations below 2-cm depth [*Dibb et al*., 2004, *Erbland et al*., 2013, *Frey et al*., 2009, *Mayewski and Legrand*, 1990, *Rothlisberger et al*., 2000], while in Greenland, surface snow layers are at most 2 times higher compared to sub-surface snow layers [*Dibb et al*., 2007]. In this study, NO_3^- concentrations in the top 2 cm of snow ($[NO_3^-]_{top}$) in Antarctica are calculated by enhancing $[NO_3^-]_{bot}$ by a factor of 6 in the top 2 cm of snow, which is the median of observed NO_3^- enhancement factors (*EF*) in Antarctica [*Dibb et al*., 2004, *Erbland et al*., 2013, *Frey et al*., 2009, *Mayewski and Legrand*, 1990, *Rothlisberger et al*., 2000]. Since NO_3^- concentrations in Antarctica are enhanced by a factor of 6 in the top 2 cm of snow, an equal amount of NO_3^- has been removed from the remainder of the photic-zone depth to maintain mass balance of NO_3^- within the snow column. In the modeled Greenland snowpack, $[NO_3^-]_{top}$ is not enhanced (*EF*=1) although *EF* is varied in a sensitivity study to assess the impact of *EF* on snow-sourced NO_x in Greenland (section 3.7).

As mentioned in the introduction, the measured quantum yields for the dominant NO_3^- photolysis pathway (E1) range from 0.003 molec $photon^{-1}$ [*Chu and Anastasio*, 2003] to 0.6 molec $photon^{-1}$ [*Zhu et al*., 2010] at T=253K and exhibit a dependency on temperature (see temperature-dependent equation in Chu and Anastasio [2003]). A higher fraction of NO_3^- was likely present on ice surfaces in the Zhu et al. [2010] study compared to the Chu and Anastasio [2003] study due to the different sample preparation methods, and likely explains the 3 order-of-magnitude difference in quantum yields. This interpretation suggests NO_3^- on the surface of ice grains is much more photolabile compared to NO_3^- embedded within ice grains, consistent with results from Meusinger et al. [2014]. In this study, we assume that NO_3^- that is wet deposited to the snow surface is more likely to be embedded in the interior of a snow grain compared to NO_3^- that is dry deposited to the surface of the snow grain. To simulate this effect in an idealized snowpack, we do not adjust the quantum yields, but instead scale snow NO_3^- concentrations by the fraction of dry relative to total (wet + dry) deposition to the Antarctic and Greenland snow surface, assuming that only the fraction of dry deposited NO_3^- is photolabile (F_p). The degree of migration of NO_3^- within a snow grain after

deposition due to snow metamorphism is unknown, which may influence the photolability of NO_3^- [*Domine and Shepson*, 2002].

Other modeling studies have attempted to calculate the fraction of photolabile NO_3^- in snow by estimating the concentration of NO_3^- contained within the liquid-like region (LLR) on the surface of ice grains (e.g., *Thomas et al*., 2012). In this work, we do not explicitly calculate NO_3^- photolysis within the LLR because there are still many unknowns about the LLR [*Domine et al*., 2013], including the distribution of NO_3^- between the bulk snow and the LLR. This distribution is better understood for some species, such as chloride [*Cho et al*., 2002], but it is unclear if NO_3^- behaves similarly. In this study, we have assumed that all NO_x formed from the photolysis of photolabile NO_3^- is transferred to the boundary layer, which neglects any recombination chemistry (e.g., Erbland et al., 2015) that prevents NO_x from leaving the ice matrix, and may lead to overestimates in the modeled F_{NOx} values presented in this study. The quantum yield for NO_3^- photolysis is dependent on the location of NO_3^- in snow, and although there are uncertainties surrounding the location of NO_3^- in snow, we perform model sensitivity studies using the full range of measured quantum yields to provide bounds for the amount of NO_x produced from snow NO_3^- photolysis.

2.2. Model Sensitivity Studies

Model results from Greenland and Antarctica are compared in section 3, which sheds light on the influence of chemical and meteorological parameters on F_{NOx}, nitrogen recycling and redistribution, and NO_3^- loss from snow. Additionally, due to uncertainties in our understanding of snow photochemistry [*Domine et al*., 2013], we perform a variety of model sensitivity studies, as shown in Table 3. The range of values used for the parameters varied in the sensitivity studies reflects our estimates of their uncertainties. The majority of these sensitivity studies focus on Antarctica, but the sensitivity of F_{NOx} to *EF* is tested in Greenland. The quantum yield is varied from 0.002 molec photon^{-1} (corresponding to T=244 K) [*Chu and Anastasio*, 2003] to 0.6 molec photon^{-1} [*Zhu et al*., 2010]. Snow NO_3^- concentrations below 2 cm ($[NO_3^-]_{bot}$) are halved and doubled with respect to the base case scenario and the impact of scaling NO_3^- concentrations by the fraction of photolabile NO_3^- (F_p) is investigated. The NO_3^- enhancement factor in the top 2 cm of snowpack is varied from 1 to 10, based upon the range of reported observations [*Dibb et al*., 2004, *Frey et al*., 2009, *Mayewski and Legrand*, 1990, *Rothlisberger et al*., 2000]. C_{BC} is halved and doubled with respect to the base case scenario. Since field and satellite measurements suggest significant increases in surface r_e throughout austral summer in Antarctica [*Jin et al*., 2008, *Klein*, 2014], the impact of increasing surface r_e during austral summer on F_{NOx} in Antarctica is evaluated in this study. The r_e profiles are varied in three sensitivity studies to examine its influence on F_{NOx}. The bulk extinction coefficient for snow ($Kext_{tot}$) is increased and decreased by 20% with respect to the base case scenario because Libois et al. [2013] suggest that the spherical snow grain assumption overestimates e-folding depths by a factor of 1.2. These sensitivity studies are used to provide estimates of the influence the uncertainty in these parameters on calculations of F_{NOx}.

2.3. Estimating the Impact of Snow NO_3^- Photolysis on Boundary Layer Chemistry and Ice-Core NO_3^- Records

NO_3^- photolysis, followed by oxidation, recycling, and redistribution of snow-sourced reactive nitrogen, influences both boundary layer chemistry and the concentration and isotopic signature of NO_3^- that is ultimately preserved in ice-core records. The preservation of NO_3^- in ice cores is most dependent on the amount of NO_3^- lost from the snow through photolysis via transport of snow-sourced NO_x away from the site of primary deposition. The methods used to explore and quantify nitrogen recycling and photolysis-driven loss of NO_3^- in snow are described in the following sections.

2.3.1. Reactive Nitrogen Recycling Between the Air and Snow

The Nitrogen Recycling Factor (*NRF)* is a metric originally proposed by Davis et al. [2008] to quantify the degree of reactive nitrogen recycling in snow over 1 year. The *NRF* is calculated in E9:

$$NRF = \frac{F_{NOx}}{F_{PRI}}, \quad \text{E9}$$

In E9, F_{NOx} (ng N m^{-2} yr^{-1}) is the annual sum of NO_x released from the snow and F_{PRI} (ng N m^{-2} yr^{-1}) is the annual sum of primary NO_3^- deposited to the snow. Davis et al. [2008] use the *NRF* to describe nitrogen recycling on both macro-scale (e.g., across the East Antarctic plateau) and micro-scale (e.g., the number of times one molecule of NO_3^- is recycled) levels. An *NRF* greater than 1 suggests that multiple nitrogen recycling events occur in the snow. *NRF* represents the average, or "bulk" degree of nitrogen recycling in snow because it does not resolve the degree of nitrogen recycling on a molecular level in the snow; some NO_3^- molecules may never be photolyzed while other NO_3^- molecules may be photolyzed and recycled many times greater than *NRF*. The *NRF* has implications for boundary layer chemistry because the continual re-emission of NO_x enhances the effective concentration of NO_x in the boundary layer [*Davis et al*., 2008]. Additionally, nitrogen recycling between the air and snow may alter the preservation of NO_3^- in ice-core records.

2.3.2. Export of Snow-sourced Nitrate Away from the Original Site of Photolysis

Once snow-sourced NO_x is emitted to the atmosphere, it is subject to transport away from the original site of photolysis. If snow-sourced NO_x is oxidized to HNO_3 and re-deposited back to the snow surface, then there is no net photolysis-driven loss of NO_3^- from the snow. However, if some of the snow-sourced NO_x is transported away from the site of primary deposition, there is a net photolysis-driven loss of NO_3^- from the snow. The fraction (*f*) of total NO_3^- (photolabile + non-photolabile) lost from the snow driven by photolysis is calculated in E10:

$$f = \left(\left(\frac{F_R}{F_{NOx}} \right)^{\tau_{NO_3^- burial}} - 1 \right) \times F_P \times F_{P_{photo}} \quad \text{E10}$$

In E10, negative values of *f* represent loss of NO_3^- from the snow and positive values of *f* represent gain of NO_3^- to the snow. In E10, F_R (ng N m^{-2} yr^{-1}) is the total annual flux of recycled NO_3^- to the snow surface and F_{NOx} (ng N m^{-2} yr^{-1}) is the total annual flux of NO_x

released from the snow from photolysis of snow NO_3^-. F_R is calculated by subtracting the depositional flux of NO_3^- from a model run without snow photochemistry from the depositional flux of NO_3^- from a model run with snow photochemistry. The ratio of F_R to F_{NOx} represents the fraction of photolabile NO_3^- remaining in the snow after 1 year. As long as NO_3^- remains in the photic zone, NO_3^- can continually be lost from the snow by photolysis-driven processes. The preservation of NO_3^- in ice cores is dependent on the fraction of NO_3^- lost from the snow through photolysis during the entire time that NO_3^- remains in the photic zone. Provided that there are no major changes in parameters that influence snow photochemistry (e.g., LAI, overhead ozone abundance) from year to year, the fraction of photolabile NO_3^- lost from the snow will be stable from year to year.

$\tau_{NO_3^-\,burial}$ represents the time that NO_3^- remains in the photic zone (years) and in E10, $\tau_{NO_3^-\,burial}$ accounts for the loss of NO_3^- that occurs during the entire time that it remains in the photic zone. When NO_3^- remains in the photic zone for less than a year ($\tau_{NO_3^-\,burial} < 1$), $\tau_{NO_3^-\,burial}$ in E10 is set equal to 1. $\tau_{NO_3^-\,burial}$ is calculated according to E11, where both the depth of the photic zone (cm) and the total annual snow accumulation (α_r) (cm yr^{-1}) are considered.

$$\tau_{NO_3^-\,burial} = \frac{z_e}{\alpha_r}, \qquad \text{E11}$$

In E11, z_e (cm) is 1 e-folding depth of UV actinic flux and is used instead of z_{3e} because 87-91% of snow-sourced NO_x is produced within the top 1 e-folding depth. To convert total annual snow accumulation rate from kg m^{-2} yr^{-1} to cm, a typical polar snow density (0.36 g cm^{-3}) [*Grenfell et al.*, 1994] is assumed. $\tau_{NO_3^-\,burial}$ is the minimum amount of time on average that NO_3^- remains in the top one-third of the snow photic zone before burial beneath because nitrogen recycling, which effectively redistributes NO_3^- upwards in the snow, is not factored into E11. $\tau_{NO_3^-\,burial}$ thus represents the lifetime of NO_3^- in snow in an average sense and does not resolve photolysis and recycling of individual NO_3^- molecules.

In E10, $\left(\left(\frac{F_R}{F_{NOx}}\right)^{\tau_{NO_3^-\,burial}} - 1\right)$ represents the fraction of photolabile NO_3^- lost from the snow through photolysis. This fraction is multiplied by F_p to calculate the fraction of total (photolabile + non-photolabile) NO_3^- lost from the snow through photolysis (f). If the lifetime of NO_3^- against burial is shorter than the lifetime of NO_3^- against photolysis, F_p is multiplied by $F_{p_{photo}}$, which represents the fraction of photolabile NO_3^- that is buried below the snow photic zone before photolysis. $F_{p_{photo}}$ is calculated in E12:

$$F_{p_{photo}} = \frac{\tau_{NO_3^-\,burial}}{\tau_{NO_3^-\,photolysis}}, \qquad \text{E12}$$

where $\tau_{NO_3^-\,burial}$ represents the lifetime of NO_3^- against burial below the photic zone and $\tau_{NO_3^-\,photolysis}$ is lifetime of NO_3^- against photolysis. $\tau_{NO_3^-\,photolysis}$ is calculated in E13:

$$\tau_{NO_3^-\,photolysis} = \frac{1}{J} \quad , \qquad \text{E13}$$

In E13, J (E8) has been integrated from λ=298-345 nm and averaged over the top e-folding depth in snow (z_e). $\tau_{NO_3^-\,photolysis}$ represents the average lifetime of NO_3^- in the snow photic zone against loss by photolysis.

If f is 0, then all snow-sourced NO_x is redeposited to the snow and there is no net loss of NO_3^-. f is also 0 if the net export of snow-sourced NO_x away from the site of original photolysis is balanced by net import of snow-sourced NO_x from other Antarctic or Greenland locations. If $-1 \leq f \leq 0$, the export of local snow-sourced NO_x is higher than the deposition of snow-sourced NO_x from elsewhere in Antarctica or Greenland, resulting in net photolysis-driven loss of NO_3^- from the snow. If $f > 0$, the export of local snow-sourced NO_x is lower than the deposition of snow-sourced NO_x from elsewhere in Antarctica or Greenland, resulting in net photolysis-driven gain of NO_3^- to the snow.

f is used to calculate the enrichment in ice-core $\delta^{15}N(NO_3^-)$ due solely to the impact of photolysis-driven loss of NO_3^- in snow when $-1 \leq f < 0$. We use a Rayleigh fractionation equation used to calculate $\delta^{15}N(NO_3^-)$ [*Blunier et al*., 2005]:

$$\delta^{15}N(NO_3^-) = ((\delta^{15}N(NO_3^-)_{air} + 1) \cdot (1+f)^{\epsilon}) - 1 \qquad \text{E14}$$

In E14, $\delta^{15}N(NO_3^-)_{air}$ is the annual-averaged $\delta^{15}N$ value of boundary layer NO_3^- and ε is the fractionation constant (-47.9‰ [*Berhanu et al*., 2014]). In this work, we set $\delta^{15}N(NO_3^-)_{air}$ equal to 0‰ to investigate the enrichment in $\delta^{15}N(NO_3^-)$ only from photolysis-driven loss of NO_3^- from snow. The model-calculated $\delta^{15}N(NO_3^-)$ enrichments represent values in snow below the photic zone (i.e., at depths where sunlight is minimal and NO_3^-photolysis is not occurring) because these values are indicative of the loss of snow NO_3^- over the total time that it spent in the snow photic zone. When NO_3^- is buried below the snow photic zone, no more photolysis or alteration of $\delta^{15}N(NO_3^-)$ occurs; hence, the $\delta^{15}N(NO_3^-)$ is further unaltered and is preserved in the ice-core record. The chemical and physical properties of snow within the photic zone are used to estimate what the enrichment in $\delta^{15}N(NO_3^-)$ would be in ice cores at depths below the snow photic zone.

3. Results and Discussion

3.1. Parameters that Influence F_{NOX} and its Spatial Redistribution

Figure 2a and 2b present modeled air temperature in the lowest vertical grid boxes, which range from 237-271 K in Antarctica and 257-280 K in Greenland; lowest temperatures are located at the highest elevations. Figure 2c and 2d show modeled total annual snow accumulation rates from GEOS-Chem (kg m^{-2} yr^{-1}), ranging from 10-700 kg m^{-2} yr^{-1} in Antarctica and 60-1400 kg m^{-2} yr^{-1} in Greenland. In both regions, the decrease in snow accumulation rate from the coast to the top of the plateau is attributed to increased distance from the ocean (moisture source), increased elevation, and lower temperatures. Figure 2e and 2f show modeled annual mean surface wind divergence from May 2009 to

May 2010. Figure 2e is consistent with Antarctic Mesoscale Prediction System surface wind output [Figure 3 in *Parish and Bromwich*, 2007], indicating that the large-scale airflow pattern in Antarctica flows from the East Antarctic plateau downslope towards the coast (katabatic winds). There are three major regions of wind convergence in Antarctica, located near the Ross, Ronne, and Amery ice shelves. In Greenland, air generally flows downwards from the continental interior towards the coasts.

Figure 3a and 3b present modeled snow C_{BC}, ranging from 0.08 to 0.6 ng g^{-1} in Antarctica and 0.8 to 5.5 ng g^{-1} in Greenland. In Antarctica, the highest C_{BC} values are found on the East Antarctic plateau and the spatial pattern of C_{BC} is governed by the snow accumulation rate; higher snow accumulation rates dilute C_{BC} [*Doherty et al.*, 2013]. The modeled boundary layer black carbon concentrations are relatively uniform across Antarctica (0.1-0.6 pptv) because the majority of black carbon reaches Antarctica through long-range transport (with the exception of local production from Antarctic research stations). In Greenland, the highest C_{BC} values are found at the coasts due to their proximity to pollution sources, even though snow accumulation rates are highest at the coasts as well. Figure 3c and 3d show mean summer (DJF, Antarctica; JJA, Greenland) e-folding depths of UV actinic flux in snow (z_e), which range from 24 to 69 cm in Antarctica and 2 to 17 cm in Greenland. The shallowest e-folding depths are located in regions of relatively high C_{BC}, which is on the plateau in Antarctica and at the coasts in Greenland. Higher C_{BC} in snow results in shallower z_e because UV absorption in snow is enhanced as the concentration of LAI increases [*Zatko et al*., 2013]. In this study, coastal grid boxes are a mixture of water, sea ice, and snow-covered surfaces, and since actinic flux profiles are only calculated for snow-covered surfaces, the average z_e in coastal grid boxes are artificially shallow.

Figure 4a and 4b show the fraction of dry-deposited NO_3^- compared to total deposited NO_3^- across Antarctica and Greenland. The ratio of dry deposition to total deposition ranges from 0.05 in coastal Antarctica and coastal Greenland to 0.92 in central Greenland and 0.99 on the East Antarctic plateau. Figure 4c and 4d show annual mean sub-surface (from 2-cm depth to the bottom of the photic zone, z_{3e}) snow NO_3^- concentrations ($[NO_3^-]_{bot}$) in the model scaled by F_p, ($[NO_3^-]_{bot}$ x F_p), which ranges from 13-60 ng g^{-1} across Antarctica and 8-121 ng g^{-1} across Greenland.

3.2. Emission, Recycling, and Redistribution of Nitrogen Across Antarctica and Greenland

Figure 5 shows model-calculated mean summer snow-sourced NO_x flux, $\overline{F_{NOx}}$, across Antarctica and Greenland. The spatial patterns of $\overline{F_{NOx}}$ in Figure 5 are governed by the depth of the photic zone (z_e) (especially in Antarctica) and also the concentration of photolabile NO_3^- (Figure 4a and 4b), which is lowest at the coasts in both Antarctica and Greenland in the model. Additionally, spatial patterns of $\overline{F_{NOx}}$ are influenced by the temperature-dependent quantum yield; the highest quantum yield values are located at the coasts where temperatures are highest. $\overline{F_{NOx}}$ ranges from 0.01-6.4x10^8 molec cm^{-2} s^{-1} in Antarctica and 0.5-11x10^8 molec cm^{-2} s^{-1} in Greenland.

Figure 6a and 6b present the total annual depositional flux of primary NO_3^- (F_{PRI}), which ranges from 0.9-35x10^5 ng N m^{-2} yr^{-1} in Antarctica and 14-1000x10^5 ng N m^{-2} yr^{-1} in Greenland and is highest at the coasts due to its relative proximity to NO_x-source regions in lower latitudes. An adjoint modeling study by Lee et al. [2014] suggests that boundary layer NO_3^- abundance in Antarctica is dominated by NO_3^- transport to Antarctica originating from NO_x emissions from 25-65°S during austral winter and by thermal decomposition of peroxyacyl nitrate (PAN) as it descends from the free troposphere in all other seasons. In Greenland, boundary layer nitrate is predominately in the gas-phase (HNO_3) [*Bergin et al*., 1995, *Dibb et al*., 1994] and it has been suggested that NO_3^- in Greenland snow originates from both the troposphere [*Geng et al*., 2014a, *Wespes et al*., 2012] and stratosphere [*Davidson et al*., 1989].

Figure 6c and 6d show the total annual depositional flux of recycled NO_3^- (F_R), which ranges from 0.5-11x10^5 ng N m^{-2} yr^{-1} in Antarctica and 0.4-9x10^5 ng N m^{-2} yr^{-1} in Greenland and is highest in areas of wind convergence (Greenland coasts and Antarctic ice shelves). Figure 6e shows the ratio of deposition of recycled nitrogen (F_R) to total deposition ($F_{PRI} + F_R$) in Antarctica. In Antarctica, recycled nitrogen (F_R) is the dominant (50-85%) form of NO_3^- deposition along the Transantarctic mountains and in regions of wind convergence, such as the Ronne, Ross, and Amery ice shelves. Along the Antarctic coast, F_R represents as little as 11% of the deposition flux. Figure 6f shows the ratio of total annual primary NO_3^- deposition to total NO_3^- deposition (primary + recycled) in Greenland. Primary NO_3^- deposition is responsible for at least 85% of total NO_3^- deposition across most of Greenland, and up to 100% in southern Greenland. This ratio is set equal to 0 over the ocean and sea ice, which leads to artificially low ratios at the coast because the model grid boxes at the coasts are an average of ocean, sea-ice, and continental values.

Figure 7 shows the Nitrogen Recycling Factor (*NRF*), which ranges from 0.2 to 12 across Antarctica and 0.01-1.6 across Greenland. Nitrogen is recycled multiple times over the course of 1 year across most of Antarctica, with the exception of the coasts. In contrast, *NRF* values are less than 1.5 across all of Greenland. The spatial pattern of *NRF* is governed by the flux of snow-sourced NO_x, which is influenced by the depth of the photic zone (z_e), the concentration of photolabile NO_3^-, and the temperature-dependent quantum yield for NO_3^- photolysis. The spatial pattern of *NRF* is also dependent on F_{PRI}, which is highest at the coasts and lowest at the top of the plateaus. In both Antarctica and Greenland, *NRF* values are lowest near the coast because the fraction of photolabile NO_3^- is small and F_{PRI} values are high. The maximum *NRF* values generally occur in regions corresponding to maximum F_{NOx} values. The average *NRF* value presented in Erbland et al. [2015] for Dome C is 4, and the difference in model-estimates of nitrogen recycling at Dome C in Erbland et al. [2015] and in this study (*NRF* = 6 at Dome C) is at least partially due to the assumption in Erbland et al. [2015] that 20% of snow-sourced NO_3^- is transported away from Dome C via katabatic winds. In GEOS-Chem, 25% of snow-sourced NO_3^- is transported away at Dome C, which is slightly larger than the assumption in Erbland et al. [2015]. Larger NO_3^- export fractions will lead to larger loss of snow NO_3^-, which may also lead to a larger number of recycling events via transport and re-deposition of snow-sourced NO_x throughout East Antarctica. Davis et al. [2008] estimate

an *NRF* of 1.8, which is roughly 3 to 6 times lower than the modeled East Antarctic *NRF* values in this study (*NRF*=5-10), although Davis et al. state that their estimated *NRF* value could be factors of 3 to 5 times higher due to uncertainties in primary nitrogen deposition estimates. Erbland et al. [2015] found a relationship between inverse snow accumulation rates and nitrogen recycling in regions where the snow accumulation rates (α_r) are higher than 50 kg m^{-2} a^{-1} in Antarctica. The relationship between *NRF* and $1/\alpha_r$ in our model simulations for α_r > 50 kg m^{-2} a^{-1} in Antarctica suggests that only 22% of the spatial variability of *NRF* can be explained by α_r (Figure S1), likely due to the redistribution of snow-sourced reactive nitrogen across Antarctica by winds. In Greenland, which is a region where snow accumulation rates are greater than 50 kg m^{-2} a^{-1}, our model simulations suggest that only 30% of the spatial variability of *NRF* can be explained by α_r (Figure S2).

3.3. Impact of Reactive Nitrogen Recycling on Boundary Layer Chemistry

The height of the boundary layer will strongly influence the abundance of NO_3^-, reactive nitrogen oxides, and oxidants emitted or formed at or near the surface. At many polar stations (e.g., Neumayer, South Pole, Dome C, Halley, Kohnen, Summit) there is a wide range of observed boundary layer heights during summer (10-600 m [*Casasanta et al*., 2014, *Cohen et al*., 2007, *Davis et al*., 2004, *Drue and Heinemann*, 2007, *Handorf*, 1996, *Helmig et al*., 2002, *Jones et al*., 2006, 2008, *King et al*., 2006, *Kodama et al*., 1985, *Konig-Langlo et al*., 1998, *Neff et al*., 2008, *Oncley et al*., 2004, *Travouillon et al*., 2008, *Weller et al*., 1999]), and although modeled boundary layer heights are not systematically biased in one direction compared to observations, they often do not agree well. Therefore, only the relative impacts of snow photochemistry on reactive nitrogen and oxidant abundances are evaluated in this study. The impact of snow NO_3^- photolysis on boundary layer chemistry can be examined by considering factor changes in boundary layer NO_x, NO_3^-, OH, and O_3 mixing ratios between simulations with and without snow NO_3^- photolysis. Other snow photochemical reactions mentioned in the introduction but not included in this modeling study will also impact oxidant abundances, but the effects of each photochemical reaction are not additive due to the highly non-linear nature of oxidant cycling.

As shown in Figure 8, the inclusion of a snow NO_x source leads to factor increases in boundary layer mixing ratios of NO_x from 1.2-24.5, gas-plus aerosol-phase nitrate from 1.0-11.8, OH from 1.8-5.3, and O_3 from 1.1-1.8 in Antarctica. The largest factor increases are in West Antarctica, particularly near the Ross and Ronne ice shelves, where winds carrying photo-produced species converge. The surface transport pattern is especially important for the redistribution of the longer-lived species NO_3^- and O_3. Figure 9 shows that the inclusion of a snow NO_x source leads to factor increases in boundary layer mixing ratios of NO_x from 1.0-6.3, gas-plus aerosol-phase nitrate from 1.0-2.2, OH from 1.1-2.4, and O_3 from 1.0-1.14 in Greenland. The largest factor increases for short-lived species (NO_x and OH) are in central Greenland where F_{NOx} is highest (Figure 5) while the largest factor increases for longer-lived species (NO_3^- and O_3) are located in regions of wind convergence.

3.4. Implications for Ice-Core Records of NO_3^- Concentrations and Isotopes

Figure 10a and 10b show the minimum amount of time that snow NO_3^- remains in the photic zone on average, $\tau_{NO_3^-\,burial}$ (E11) as calculated in the model. NO_3^- remains in the snow photic zone for 4 months near the Antarctic coasts and up to 6.5 years on the East Antarctic plateau before burial below the photic zone. In Greenland, NO_3^- remains in the photic zone for 0.1 months at the coasts and up to 7 months in central Greenland. The spatial pattern of $\tau_{NO_3^-\,burial}$ is governed by the snow accumulation rate, both directly and indirectly through its influence on C_{BC}. The spatial patterns of $\tau_{NO_3^-\,burial}$ are in agreement with the expectation that NO_3^- remains in the photic zone the longest in areas with low snow accumulation rates.

In Antarctica, the lifetime of NO_3^- against burial is always longer than the lifetime of NO_3^- against photolysis. However in Greenland, the lifetime of NO_3^- against burial may be shorter than the lifetime against photolysis due to the much shorter $\tau_{NO_3^-\,burial}$ values. Figure 10c presents the lifetime of nitrate against photolysis in Greenland ($\tau_{NO_3^-\,photolysis}$, E13), which ranges from less than a month in northern Greenland to 37 months in southern Greenland. The spatial pattern of $\tau_{NO_3^-\,photolysis}$ is dependent on the mean summer (JJA) daily-averaged downwelling surface irradiance values (not shown), which are highest in northern Greenland. Figure 10d shows $F_{p_{photo}}$ (E12), which ranges from 0.003 to 1 across Greenland. Larger $F_{p_{photo}}$ values in north-central Greenland suggest that the lifetime of photolabile NO_3^- against photolysis is sufficiently short relative to its lifetime in the snow photic zone, allowing for a potentially large fraction of snow NO_3^- to be photolyzed before burial beneath the photic zone. In southeastern Greenland, the lifetime of photolabile NO_3^- against photolysis is longer than its lifetime in the snow photic zone, which will reduce post-depositional photolysis of snow NO_3^- in this region.

Figure 11a and 11b show the fraction of NO_3^- gained or lost from the snow through photolysis (*f,* E10), which ranges from -0.99 to 0.30 in Antarctica and -0.83 to 0.02 in Greenland. Throughout most of Antarctica and Greenland, values of *f* are negative indicating that the photolysis of snow NO_3^- leads to net loss of NO_3^- from the snowpack in most locations. Positive *f* values indicate regions with net gain of NO_3^- to the snow resulting from the spatial redistribution of NO_3^- driven by snow photochemistry. In some regions of convergence, such as over the Ronne Ice Shelf in Antarctica, there is a net gain of snow-sourced NO_3^-. There are sharp gradients in *f* between the plateaus and the coasts. The largest loss of snow NO_3^- occurs at the top of the plateaus, where most photolyzed NO_3^- is transported away by katabatic winds. Along the coasts, the photolysis-driven loss of NO_3^- from the snow is minimal due to high snow accumulation rates and transport of snow-sourced NO_3^- from higher elevations. The spatial pattern of *f* is influenced by the time that NO_3^- remains in the photolytic zone ($\tau_{NO_3^-\,burial}$), the concentration of photolabile NO_3^- (F_p), and wind patterns across Antarctica and Greenland.

Figure 11c and 11d show modeled enrichments in ice-core $\delta^{15}N(NO_3^-)$ from photolysis-driven loss of NO_3^- in snow. The $\delta^{15}N(NO_3^-)$ enrichments presented in Figures 11c and 11d represent enrichments in $\delta^{15}N(NO_3^-)$ below the snow photic zone where NO_3^-

photolysis is not occurring, effectively integrating the total loss of NO_3^- during its lifetime in the snow photic zone. Model-calculated ice-core $\delta^{15}N(NO_3^-)$ values range from 0 to 363‰ in Antarctica and 0 to 90‰ in Greenland and are highest at the tops of the plateaus. The modeled ice-core $\delta^{15}N(NO_3^-)$ enrichments resulting from the photolysis-driven loss of snow nitrate are sensitive to the fractionation constant (ε). In this study, the fractionation constant is varied over the full range of values reported in Erbland et al [2013], Frey et al., [2009], and Shi et al. [2015]; an ε of –90‰ increases modeled ice-core $\delta^{15}N(NO_3^-)$ by a factor of 2 and an ε of -10‰ decreases modeled ice-core $\delta^{15}N(NO_3^-)$ by a factor of 5 across Antarctica and Greenland.

3.5. Relationship Between Nitrogen Recycling and Photolytic-loss of NO_3^- in Snow

The degree of photolysis-driven loss of snow NO_3^- is determined by both rates of photolysis and transport patterns across Antarctica and Greenland. The spatial patterns of recycling (*NRF*, Figure 7) and loss (*f*, Figure 11a and 11b) differ across Antarctica and Figure 12 shows the relationship between *f* and *NRF* across Antarctica. The magnitude of nitrogen recycling and degree of photolysis-driven loss of snow NO_3^- in Antarctica are well correlated ($r^2 = 0.74$, $p < 0.001$) in regions where NO_3^- remains in the photic zone for less than 2 years ($\tau_{NO_3^-\,burial} < 2$) (Figure 12a). The relationship between recycling and loss breaks down ($r^2 = 0.03$, $p < 0.001$) in locations where NO_3^- remains in the photic zone for more than 2 years (Figure 12b). The relationship between recycling and loss weakens with increasing $\tau_{NO_3^-\,burial}$ because recycling of reactive nitrogen occurs at or near the surface only, while loss of NO_3^- occurs throughout the depth of snow photic zone. The time that NO_3^- remains in the snow photic zone is dependent on snow accumulation rates and the concentrations of LAI in snow, the latter of which is partially governed by snow accumulation rates. In the present climate, $\tau_{NO_3^-\,burial}$ less than 2 years corresponds to snow accumulation rates higher than 130 kg m^{-2} a^{-1} in Antarctica. Figure 13 shows the relationship between *f* and *NRF* in Greenland. Nitrogen recycling and the degree of photolysis-driven loss of snow NO_3^- are well correlated ($r^2 = 0.71$, $p < 0.001$) in Greenland, likely because NO_3^- remains in the photic zone for less than 2 years across all of Greenland. Snow accumulation rates are higher than 130 kg m^{-2} a^{-1} across much of Greenland, except in parts of central Greenland, where snow accumulation rates are between 60 and 100 kg m^{-2} a^{-1}. Differences in the relationship between snow accumulation rate and $\tau_{NO_3^-\,burial}$ between Greenland and Antarctica are due to the higher concentrations of LAI in Greenland snow.

3.6. Comparison between Greenland and Antarctica

Comparing model results in Greenland and Antarctica reveals information about how different parameters influence snow-sourced NO_x fluxes, nitrogen recycling, and photolysis-driven loss of snow NO_3^-. Air temperatures (Figure 2a, 2b) and annual snow accumulation rates (Figure 2c, 2d) are generally higher in Greenland compared to Antarctica, and Greenland is also closer to pollution sources, which lead to differences in the magnitudes and spatial patterns of F_{NOx}, *NRF*, and *f* between these two regions.

The magnitude and spatial patterns of F_{NOx} are influenced by snow photic zone depths (which are governed by snow LAI concentrations), snow NO_3^- concentrations, and the

quantum yield for NO_3^- photolysis. The e-folding depths of UV actinic flux are shallower in Greenland (2-17 cm) compared to Antarctica (24-69 cm) because concentrations of light-absorbing impurities in snow are higher in Greenland (C_{BC} = 0.8-5.5 ng g^{-1}) compared to Antarctica (C_{BC} = 0.08-0.6 ng g^{-1}). Similar to snow C_{BC}, the proximity of Greenland to natural and anthropogenic NO_x sources leads to higher observed snow NO_3^- values; the median of observed sub-surface snow NO_3^- concentrations in Greenland (132 ng g^{-1}, [*Burkhart et al*., 2009]) is over 2 times higher than observed sub-surface snow NO_3^- concentrations in Antarctica (60 ng g^{-1}, [*Bertler et al*., 2005]). Similarly, modeled sub-surface snow NO_3^- concentrations ($[NO_3^-]_{bot}$ x F_p) are higher across much of Greenland compared to Antarctica. However, in coastal Antarctica and Greenland, modeled sub-surface snow NO_3^- concentrations ($[NO_3^-]_{bot}$ x F_p) are similar in magnitude because the fraction of dry-deposited NO_3^- to total deposited NO_3^- (F_p) is lower in Greenland, which lowers the concentration of photolabile NO_3^- in the model. Additionally, modeled snow NO_3^- in the top 2 cm of snow ($[NO_3^-]_{top}$) is generally higher across Antarctica ($[NO_3^-]_{top}$=78-360 ng g^{-1}) compared to Greenland ($[NO_3^-]_{top}$=8-121 ng g^{-1}) because EF=6 in Antarctica and EF=1 in Greenland. Lastly, summer temperatures are higher in Greenland (257-280 K) compared to Antarctica (237-271 K), which leads to higher quantum yields for NO_3^- photolysis in Greenland (ϕ=0.0032-0.0069) compared to Antarctica (ϕ=0.0015-0.0052).

Fluxes of snow-sourced NO_x (F_{NOx}) are somewhat higher in Greenland (0.5-11x10^8 molec cm^{-2} s^{-1}) compared to Antarctica (0.01-6.4x10^8 molec cm^{-2} s^{-1}) because ϕ, and often sub-surface snow NO_3^- concentrations ($[NO_3^-]_{bot}$ x F_p), are higher in Greenland compared to Antarctica, even though snow photic zones are shallower across Greenland due to higher snow LAI concentrations. In Antarctica, the highest F_{NOx} values occur midway up the plateau because photic zone depths and the quantum yields for NO_3^- photolysis increase towards the coast while the concentrations of photolabile NO_3^- decrease towards the coast. In Greenland, the highest F_{NOx} values occur at the top of the plateau because both photic zone depths and concentrations of photolabile NO_3^- are at a maximum there. The quantum yield of NO_3^- photolysis increases towards the coast, partially dampening the decreasing F_{NOx} gradient towards the coast.

The Nitrogen Recycling Factors (*NRF*) are much smaller in Greenland (*NRF*=0.01-1.6) compared to Antarctica (*NRF*=0.2-12), suggesting that the degree of nitrogen recycling is much lower in Greenland. Although F_{NOx} values are generally higher in Greenland compared to Antarctica, the degree of nitrogen recycling is lower in Greenland because of its proximity to pollution sources. Primary deposition of NO_3^- is over an order of magnitude larger in Greenland compared to Antarctica. The total nitrate, NO_x, OH, and O_3 boundary layer mixing ratio factor increases in Greenland are 16, 7, 3, and 2 times lower, respectively, compared to Antarctica due to its proximity to pollution sources.

NO_3^- remains in the snow photic zone for a shorter period of time in Greenland (up to 7 months) compared to Antarctica (up to 6.5 years), because photic zones are shallower and snow accumulation rates are higher in Greenland. The assumed fraction of photolabile NO_3^- (F_p) in the model is lower in Greenland compared to Antarctica because a higher fraction of NO_3^- is wet-deposited in Greenland. Additionally, the lifetime of photolabile

NO_3^- against burial beneath the snow photic zone ($\tau_{NO_3^-\ burial}$) is generally shorter than its lifetime against photolysis ($\tau_{NO_3^-\ photolysis}$) in Greenland, further limiting post-depositional loss and recycling of snow NO_3^-.

In both Greenland and Antarctica, the highest fractions of photolysis-driven loss of snow NO_3^- (*f*) are located at the top of the plateaus and the lowest *f* values are found at the coasts. Photolysis-driven loss of snow NO_3^- is generally lower in Greenland compared to Antarctica because the fraction of photolabile NO_3^- (F_p) and the time spent in the snow photic zone ($\tau_{NO_3^-\ burial}$) are lower in Greenland. Similar to the spatial patterns of *f*, modeled enrichments in ice-core $\delta^{15}N(NO_3^-)$ are highest on the plateau and lowest at the coasts in both Antarctica and Greenland. $\delta^{15}N(NO_3^-)$ values in Antarctica are up to 4 times larger compared to Greenland because a higher fraction of NO_3^- is lost from the snow via photolysis in Antarctica.

3.7. Exploring the Influence of Chemical, Optical, and Physical Parameters in Snow on F_{NOx}

Snow accumulation rates have a major influence on snow-sourced NO_x fluxes, nitrogen recycling and redistribution, and photolysis-driven loss of snow NO_3^- via two mechanisms. By impacting burial rates, the snow accumulation rate impacts the time NO_3^- spends in the snow photic zone. Snow accumulation rates influence light-absorbing impurity concentrations in snow, which impact the depth of the snow photic zone. Snow accumulation rates also influence concentrations of photolabile NO_3^- in snow; both directly through dilution effects and indirectly by controlling the partitioning of wet and dry deposited NO_3^-. Temperature also influences F_{NOx} via the temperature-dependent quantum yield (ϕ), with higher temperatures leading to higher values of ϕ.

In addition to exploring the sensitivity of snow NO_3^- photolysis to meteorological parameters, the sensitivity of mean summer snow-sourced NO_x fluxes ($\overline{F_{NOx}}$) to a variety of chemical, optical, and physical parameters in snow is explored in this section. Although the vast majority of these sensitivity studies focus on Antarctica because model computation time was limited, one sensitivity study was performed in Greenland and will be described below.

Table 3 shows the dependence of $\overline{F_{NOx}}$ on uncertainties in the quantum yield for NO_3^- photolysis (ϕ), the fraction of photolabile NO_3^- (F_p), sub-surface snow NO_3^- concentrations ($[NO_3^-]_{bot}$), radiation equivalent mean ice grain radii (r_e), the bulk snow extinction coefficient ($Kext_{tot}$), the NO_3^- concentration enhancement factor in the top 2 cm of snow (*EF*), and snow black carbon concentrations in Antarctica. The range of values for each of these parameters is determined by their estimated degree of uncertainty, in order to highlight the largest uncertainties in calculations of $\overline{F_{NOx}}$. The sensitivity study results are compared to $\overline{F_{NOx}}$ from the standard scenario, which is also described in Table 3. The $\overline{F_{NOx}}$ values from the standard scenario are slightly different than the $\overline{F_{NOx}}$ values presented in Figure 5a because a spatially-uniform ϕ is used in the standard scenario while a temperature-dependent ϕ is used in the rest of the manuscript (Figures 5-14).

$\overline{F_{NOx}}$ is most sensitive to uncertainties in ϕ, which increases $\overline{F_{NOx}}$ by up to a factor of 330 when ϕ from Zhu et al. [2010] (0.6 molec photon^{-1}) is used compared to the ϕ in the standard scenario (ϕ=0.002 molec photon^{-1} [*Chu and Anastasio*, 2003]). The second most influential parameter is the concentration of photolabile NO_3^- ($[NO_3^-]_{bot}$ x F_p). Assuming that all NO_3^- is photolabile (F_p=1) increases $\overline{F_{NOx}}$ by up to a factor of 7.4 (at the coasts) with respect to the standard scenario. Use of the fraction of dry-deposited NO_3^- (F_p) to scale the concentration of photolabile NO_3^- lowers $\overline{F_{NOx}}$ by up to 85% along the coast, but has little impact on the East Antarctic plateau due to the high fraction of dry deposited NO_3^-. Uncertainties in r_e, $Kext_{tot}$, EF, and C_{BC} influence $\overline{F_{NOx}}$ by up to a factor of 1.3 compared to the standard scenario. In Greenland, EF is varied between 1 and 2, which is the range of observed EF presented in Dibb et al. [2007]. Similar to Antarctica, varying EF from 1 to 2 increases $\overline{F_{NOx}}$ in Greenland by at most a factor of 1.2.

Calculated snow-sourced NO_x fluxes are by far most sensitive to uncertainties in the quantum yield for NO_3^- photolysis and the concentration of photolabile NO_3^-, which are likely related to one another. The results of Chu et al. [2003], Zhu et al. [2010], and Meusinger et al. [2014] suggest that the quantum yield is largely influenced by the location of NO_3^- in the ice grain; quantum yields tend to be lowest when NO_3^- is buried within the ice grain and highest when NO_3^- is on the ice grain surface. Although we have not explicitly varied the quantum yield based upon NO_3^- location in ice grains due to lack of information regarding the location, we alter the concentration of photolabile NO_3^- based upon the ratio of dry to total deposited NO_3^- This effectively assumes that only the dry-deposited fraction of NO_3^- is on the surface of the snow grain and is photolabile, and that the wet-deposited NO_3^- is trapped within an ice grain and thus is not photolabile. Using conservative ϕ values (Chu and Anastasio, [2003]) and assuming that only dry-deposited NO_3^- is photolabile may suggest that our calculated F_{NOx} values represent a lower limit. However, no field-or laboratory-based information is available to assess our assumption that only dry-deposited NO_3^- is photolabile; it is possible that the fraction of NO_3^- that is photolabile is higher or lower than what we assume.

These sensitivity studies highlight the need for field, laboratory, and modeling studies to investigate factors influencing the quantum yield and concentration of photolabile NO_3^-, such as the location of NO_3^- within ice grains. We note that F_{NOx} is also sensitive to the depth of the snow photic zone, which in turn is most sensitive to snow LAI concentrations and r_e [*Zatko et al*., 2013]. By scaling the concentrations of total snow LAI to C_{BC} in the model based on observations in Greenland and Antarctica [*Zatko et al*., 2013], we assume the same factor of 2 uncertainty in total LAI concentrations as we do for C_{BC}. More measurements of snow LAI other than black carbon are needed to confirm our assumptions about snow LAI concentrations and their associated uncertainty.

4. Conclusions

We have incorporated an idealized snowpack along with a snow radiative transfer model into a global chemical transport model (GEOS-Chem) and used this modeling framework to simulate the photolysis of snow NO_3^- and calculate the associated snow-sourced flux and redistribution of nitrogen across Antarctica and Greenland. An important goal of this study is to explore the sensitivity of various chemical, optical, and physical properties of

snow, as well as meteorology, on fluxes of snow-sourced NO_x and related nitrogen recycling, redistribution, and loss of NO_3^- from the snow. This modeling framework is also used to examine the impact of snowpack NO_3^- photolysis on boundary layer chemistry and the preservation of NO_3^- concentration and nitrogen isotopes in ice cores across Antarctica and Greenland.

The calculated fluxes of snow-sourced NO_x in Antarctica and Greenland range from 0.01-6.4x10^8 molec cm^2 s^{-1} and 0.5-11x10^8 molec cm^2 s^{-1}, respectively. The modeled spatial patterns of snow-sourced NO_x fluxes are determined by the spatial patterns of light-absorbing impurity (e.g., insoluble black carbon, dust, organics) concentrations in snow, photolabile NO_3^- concentrations, and temperature-dependent quantum yields for NO_3^- photolysis. In the model, the spatial patterns of light-absorbing impurities are influenced by snow accumulation rates and proximity to pollution sources, the spatial patterns of photolabile NO_3^- in the model are influenced by the amount of wet-deposited NO_3^- compared to total deposited NO_3^-, and the spatial patterns of quantum yields of NO_3^- photolysis are influenced by modeled surface air temperatures. Model sensitivity studies suggest that the magnitude of the snow-sourced NO_x flux is most sensitive to uncertainties in the quantum yield for NO_3^- photolysis and the concentration of photolabile NO_3^-, which are likely related to one another. The concentration of light absorbing impurities in snow is also important for the flux of snow-sourced NO_x, but we assume a much smaller degree of uncertainty in this parameter relative to uncertainties in the quantum yield and the concentrations of photolabile NO_3^-. Fluxes of snow-sourced NO_x are somewhat higher in Greenland compared to Antarctica because the quantum yields, and often photolabile NO_3^- concentrations, are higher in Greenland because Greenland is warmer and closer to anthropogenic NO_x sources (e.g., northern hemisphere mid-latitudes). This is counteracted by the higher concentrations of snow light-absorbing impurities leading to shallower show photic zones in Greenland.

The Nitrogen Recycling Factor (*NRF*) is dependent on the magnitude and spatial patterns of fluxes of primary NO_3^- to the snow relative to fluxes of NO_x from the snow. *NRF* values greater than 1 suggest that nitrogen is recycled multiple times between the air and snow. *NRF* values range from 0.2 to 12 in Antarctica and are greater than 1 across most of Antarctica, with the exception of the coasts. *NRF* values range from 0.01 to 1.6 in Greenland and are only larger than 1 in central Greenland. The degree of nitrogen recycling is lower in Greenland because NO_3^- deposition to snow is dominated by primary NO_3^- deposition in Greenland, largely because Greenland is closer to pollution sources. Similarly, boundary-layer mixing ratios of total nitrate, NO_x, OH, and O_3 are less influenced by snow-sourced NO_x in Greenland because of its proximity to pollution sources.

This modeling framework can also be used to examine the impact of NO_3^- photolysis on the preservation of NO_3^- in ice cores. The time that NO_3^- remains in the snow photic zone is dependent on snow accumulation rates both directly, and indirectly through their influence on light-absorbing impurity concentrations in snow. NO_3^- remains in the snow photic zone for a much shorter period of time in Greenland (up to 7 months) compared to Antarctica (up to 6.5 years) because snow accumulation rates are higher in Greenland.

The fraction of NO_3^- lost from the snow through photolysis (*f*) ranges from -0.99 to 0.30 in Antarctica and -0.83 to 0.02 in Greenland, where negative values indicate net loss of NO_3^- from the snow. The fraction of NO_3^- lost from the snow is dependent on the time that NO_3^- remains in the snow photic zone, the concentration of photolabile NO_3^-, and wind patterns across Antarctica and Greenland. In both Antarctica and Greenland, net loss of snow NO_3^- is highest on top of the plateaus and lowest at the coasts; some regions (e.g., Ronne and Ross Antarctic ice shelves) experience net gain of snow NO_3^- due to the redistribution of snow-sourced nitrogen. The fraction of photolysis-driven loss of snow NO_3^- is lower in Greenland compared to Antarctica because the fraction of photolabile NO_3^- and the time spent in the snow photic zone ($\tau_{NO_3^-\,burial}$) is lower in Greenland due to the higher snow accumulation rates and higher concentrations of snow light absorbing impurities. The fraction of NO_3^- lost from the snow through photolysis is used to calculate the enrichment in ice-core $\delta^{15}N(NO_3^-)$ solely from photolysis-driven NO_3^- loss in snow. The modeled enrichment in ice-core $\delta^{15}N(NO_3^-)$ ranges from 0 to 363‰ in Antarctica and 0 to 90‰ in Greenland; the highest $\delta^{15}N(NO_3^-)$ enrichments are calculated in central Antarctica and Greenland.

A significant relationship exists between nitrogen recycling and photolysis-driven loss of snow NO_3^- in Antarctica when NO_3^- remains in the photic zone for less than 2 years ($\tau_{NO_3^-\,burial} < 2$), corresponding to a snow accumulation rate greater than 130 kg m^{-2} a^{-1} in the present day. There is also a significant relationship between nitrogen recycling and photolysis-driven loss of snow NO_3^- throughout all of Greenland, which is a region where snow accumulation rates are generally higher than 130 kg m^{-2} a^{-1}. Since the spatial variability of ice-core $\delta^{15}N(NO_3^-)$ is mainly determined by the fractional loss of snow NO_3^- due to the large fractionation factor associated with its photolysis [*Berhanu et al*., 2014], observations of $\delta^{15}N(NO_3^-)$ in snow and ice can be used to estimate both the degree of recycling and loss of snow NO_3^- in Antarctica and Greenland as long as this condition is met. The relationship between recycling and loss can be useful for the interpretation of the oxygen isotopic composition of ice-core NO_3^- (e.g., Sofen et al. [2014]), which is impacted by recycling of snow NO_3^-. We note that the relationship between $\tau_{NO_3^-\,burial}$ and snow accumulation rate may vary in different climates depending on the concentrations of light-absorbing impurities in snow [*Geng et al*., 2015].

This is the first modeling study to incorporate an idealized snowpack along with a snow radiative transfer model into a global chemical transport model. This modeling framework is used to investigate the impacts of snow-sourced NO_x on boundary layer chemistry and nitrogen recycling and redistribution, and its spatial variability, across Antarctica and Greenland. The modeled spatial patterns of nitrogen recycling, photolysis-driven loss of NO_3^- from snow, and ice-core $\delta^{15}N(NO_3^-)$ are each sensitive to multiple meteorological and chemical parameters, some of which are interdependent. Model sensitivity studies suggest that future field, laboratory, and modeling studies continue to focus on gaining a better understanding of the quantum yield for NO_3^- photolysis and the concentration of photolabile NO_3^-, which are likely related. More observations of the concentration of UV light absorbing impurities in snow are also needed. Updated information about the quantum yield for NO_3^- photolysis and the concentration of photolabile NO_3^- in snow along with additional snow photochemical reactions can be

incorporated into this modeling framework in the future, which will continue to improve our understanding of the impacts of snow photochemistry on boundary layer chemistry and the preservation of NO_3^- and other photochemically-active species in ice cores.

Acknowledgments

We acknowledge support from NSF PLR 1244817, NSF PLR 0944537, NSF PLR 1446904, and an EPA STAR graduate fellowship to M.C. Zatko. The authors thank Steve Warren, Sarah Doherty, Thomas Grenfell, and Quentin Libois for helpful discussions about light-absorbing impurities in snow and their influence on snow photochemistry. We thank Joseph Erbland for many helpful comments and discussions about nitrogen recycling. Joel Thornton and Lyatt Jaeglé also provided many helpful comments about this work. We also thank Paul Hezel and Yanxu Zhang for helping M.C. Zatko learn GEOS-Chem. We thank Qianjie Chen for helpful feedback on paper drafts and Martin Schneebeli for providing useful advice about snow grain profiles in Antarctic snow. The authors thank the editor and two anonymous reviewers for helpful comments.

References

Allen, D., Pickering, K., Duncan, B., Damon, M.: Impact of lightning NO emissions on North American photochemistry as determined using the Global Modeling Initiative (GMI) model. *J. Geophys. Res*., 115, D22301, doi:10.1029/2010JD014062, 2010.

Alexander, B., Savarino, J., Kreutz, K.J., Thiemens, M.H.: Impact of preindustrial biomass burning emissions on the oxidation pathways of tropospheric sulphur and nitrogen. *J. Geophys. Res.*, 109, D08303, doi:10.1029/2003/JD004218, 2004.

Amos, H. M., Jacob, D.J, Holmes, C.D, Fisher, J.A, Wang, Q., Yantosca, R.M., Corbitt, E.S., Galarneau, E., Rutter, A.P., Gustin, M.S., Steffen, A., Schauer, J.J, Graydon, J.A., St. Louis, V.L., Talbot, R.W., Edgerton, E.S., Zhang, Y., Sunderland, E.M.: Gas-Particle Partitioning of Atmospheric Hg(II) and Its Effect on Global Mercury Deposition, *Atmos. Chem. Phys.*, **12**, 591-603, 2012.

Anastasio, C. and Chu, L.: Photochemistry of nitrous acid (HONO) and nitrous acidium ion (H_2ONO^+) in aqueous solution and ice. *Environ. Sci. Tech*., 43, 1108-1114, 2009.

Beine, H., Anastastio, C., Esposito, G., Patten, K., Wilkening, E., Domine, F., Voisin, D., Barret, M., Houdier, S., Hall, S.: Soluble, light-absorbing species in snow at Barrow, Alaska. *J. Geophys. Res*., 116, D00R05, doi: 10.1029/2011JD016181, 2011.

Bergin, M.H., Jaffrezo, J.-L., Davidson, C.I., Dibb, J.E., Pandis, S.N., Hillamo, R., Maenhaut, M., Kuhns, H.D., Makela, T.: The contributions of snow, fog, and dry deposition to the summer flux of anions and cations at Summit, Greenland. *J. Geophys. Res*., 100(D8), 16275-16288.

Berhanu, T. A., Meusinger, C., Erbland, J., Jost, R., Bhattcharya, S. K., Johnson, M. S., Savarino, J.: Laboratory study of nitrate photolysis in Antarctic snow. II. Isotopic effects and wavelength dependence. J. Chem. Phys., 140, 244306, doi:10.1063/1.4882899, 2014.

Bertler, N., Mayewski, P. A., Aristarain, A., Barrett, P., Becagli, S., Bernardo, R., Bo, S., Xiao, C., Curran, M., Qin, D., Dixon, D., Ferron, F., Fischer, H., Frey, M., Frezzotti, M., Fundel, F., Genthon, C., Gragnani, R., Hamilton, G., Handley, M., Hong, S., Isaksson, E., Kang, J., Ren, J., Kamiyama, K., Kanamori, S., Karkas, E., Karlof, L., Kaspari, S., Kreutz, K., Kurbatov, A., Meyerson, E., Ming, Y., Zhang, M., Motoyama, H., Mulvaney, R., Oerter, H., Osterberg, E., Proposito, M., Pyne, A., Ruth, U., Simoes, J., Smith, B., Sneed, S., Teinila, K., Traufetter, F., Udisti, R., Virkkula, A., Watanabe, O., Williamson, R., Winther, J-G., Li, Y., Wolff, E., Li, Z., Zielinski, A.: Snow chemistry across Antarctica, *Annals of Glaciology*, *41*(1), 167- 179, 2005.

Bey, I., Jacob, D.J., Yantosca, R.M., Logan, J.A., Field, B.D., Fiore, A.M., Li, Q., Liu, H.Y., Mickley, L.J., Schultz, M.G.: Global modeling of tropospheric chemistry with assimilated meteorology: Model description and evaluation, *J. Geophys. Res.*, *106*(D19), 23073-23095, 2001.

Bian, H.S., Prather, M.J.: Fast-J2: Accurate simulation of stratospheric photolysis in global chemical models. *J. Atmos. Chem*., 41, 281-296, 2002.

Bloss, W.J., Lee, J.D., Heard, D.E., Salmon, R.A., Bauguitte, S.J-B., Roscoe, H.K., Jones, A.E.: Observations of OH and HO_2 radicals in coastal Antarctica. Atmos. Chem. Phys., 7, 4171-4185, 2007.

Boxe, C.S., Colussi, A.J., Hoffmann, M.R., Murphy, J.G., Wolldridge, P.J., Bertram, T.H., Cohen, R.C.: Photochemical production and release of gaseous NO_2 from nitrate-doped water ice. J. Phys. Chem., A, 109, 8520-8525, 2005.

Blunier, T., Gregoire, F. L., Jacobi, H.-W., and Quansah, E.: Isotopic view on nitrate loss in Antarctic surface snow. *Geophys. Res. Lett*., 32, L13501, doi:10.1029/2005GL023011, 2005.

Burkhart, J.F., Bales, R.C., McConnell, J.R., Hutterli, M.A., Frey, M.M.: Geographic variability of nitrate deposition and preservation over the Greenland ice sheet. *J. Geophys. Res*., 114(D06301), doi:10.1029/2008JD010600, 2009.

Casasanta, G., Pietroni, I., Petenko, I., Argentini, S.: Observed and modelled convective mixing-layer height in Dome C, Antarctica. *Boundary-Layer Meteorol.*, 151, 597-608, doi:10.1007/s10546-014-9907-5, 2014.

Chen, G., Davis, D., Crawford, J., Hutterli, L.M., Huey, L.G., Slusher, D., Mauldin, L., Eisele, F., Tanner, D., Dibb, J., Buhr, M., McConnell, J., Lefer, B., Shetter, R., Blake, D., Song, C.H., Lombardi, K., Arnoldy, J.: A reassessment of HO_x South Pole chemistry based on observations recorded during ISCAT 2000. *Atmos. Environ*., 38, 5451-5461, 2004.

1089 Chen, G., Huey, L.G., Crawford, J.H., Olson, J.R., Hutterli, M.A., Sjostedt, S., Tanner,
1090 D., Dibb, J., Lefer, B., Blake, N., Davis, D., Stohl, A.: An assessment of the polar HOx
1091 photochemical budget based on 2003 Summit Greenland Field Observations. *Atmos.*
1092 *Environ*., 41, 36, 7806-7820, 2007.
1093
1094 Chu, L., and Anastasio. C.: Quantum Yields of Hydroxyl Radicals and Nitrogen Dioxide
1095 from the Photolysis of Nitrate on Ice. *J. Phys. Chem*. *A*., 107, 9594-9602, 2003.
1096
1097 Cho, H., Shepson, P.B., Barrie, L.A., Cowin, J.P., Zaveri, R.: NMR Investigation of the
1098 Quasi-Brine Layer in Ice/Brine Mixtures. *J. Phys. Chem. B*., 106, 11226-11232, 2002.
1099
1100 Cohen, L., Helmig, D., Neff, W.D., Grachev, A. A., Fairall, C.W.: Boundary-layer
1101 dynamics and its influence on atmospheric chemistry at Summit, Greenland. *Atmos.*
1102 *Environ*., 41, 24, 5044-5060, 2007.
1103
1104 Davidson, C.I., Harrington, J.R., Stephenson, M.J., Small, M.J., Boscoe, F.P., Gandley,
1105 R.E.: Seasonal variations in sulfate, nitrate, and chloride in the Greenland ice sheet:
1106 relation to atmospheric concentrations. Atmos. Environ., 23(11), 2483-2493, 1989.
1107
1108 Davis, D., Chen, G., Buhr, M., Crawford, J., Lenschow, D., Lefer, B., Shetter, R., Eisele,
1109 F., Mauldin, L., Hogan, A.: South Pole NOx Chemistry: an assessment of factors
1110 controlling variability and absolute levels. *Atmos. Environ*., 38, 5375-5388, 2004.
1111
1112 Davis, D. D., Seelig, J., Huey, G., Crawford, J., Chen, G., Wang, Y., Buhr, M., Helmig,
1113 D., Neff, W., Blake, D., Arimoto, R., Eisele, F.: A reassessment of Antarctic plateau
1114 reactive nitrogen based on ANTCI 2003 airborne and ground based measurements.
1115 *Atmos. Environ*., 42, 2831-2848, doi:10.1016/j.atmosenv.2007.07.039, 2008.
1116
1117 Dibb, J.E., Talbot, R.W., Bergin, M.H.: Soluble acidic species in air and snow at Summit,
1118 Greenland. *Geophys. Res. Lett*., 21(15), 1627-1630, 1994.
1119
1120 Dibb, J. E., Huey, G. L., Slusher, D. L., and Tanner, D. J.: Soluble reactive nitrogen
1121 oxides at South Pole during ISCAT 2000. *Atmos. Environ*., 38, 5399-5409, 2004.
1122
1123 Dibb, J.E., Whitlow, S.I., Arsenault, M.: Seasonal variations in the soluble ion content of
1124 snow at Summit, Greenland: constraints from three years of daily surface snow samples.
1125 *Atmos. Environ*., 41, 5007-5019, doi:10.1016/j.atmosenv.2006.12.010, 2007.
1126
1127 Doherty, S. J., Warren, S. G., Grenfell, T. C., Clarke, A. D., and Brandt, R. E.: Light-
1128 absorbing impurities in Arctic snow. *Atmos. Chem. Phys*., 10, 11647-11680,
1129 doi:10.5194/acp-10-11647-2010, 2010.
1130
1131 Doherty, S. J., Grenfell, T.C., Forsstrom, S., Hegg, D.L., Brandt, R.E., Warren, S.G.:
1132 Observed vertical redistribution of black carbon and other insoluble light-absorbing
1133 particles in melting snow, *J*. *Geophys*. *Res*. *Atmos*., 118, 1-17, doi:10.1002/jgrd.50235,
1134 2013.

Domine, F., Shepson, P. B.: Air-snow interactions and atmospheric chemistry, *Science*, 297, 1506–1510, 2002.

Domine, F., Bock, J., Voisin, D., Donaldson, D. J.: Can we model snow photochemistry? Problems with the current approaches. *J. Phys. Chem. A*, 117, 4733-4749, doi: 10.1021/jp3123314 2013.

Drue, C., Heinemann, G.: Characteristics of intermittent turbulence in the upper stable boundary layer over Greenland. Boundary-Layer Meteorol., 124, 361-381, doi:10.1007/s10546-007-9175-8, 2007.

Erbland, J., Vicars, W.C., Savarino, J., Morin, S., Frey, M.M., Frosini, D., Vince, E., Martins, J.M.F.: Air-snow transfer of nitrate on the East Antarctic Plateau – Part 1: Isotopic evidence for a photolytically driven dynamic equilibrium in summer. *Atmos. Chem. Phys*., 13, 6403-6419, doi:10.5194/acp-13-6403-2013, 2013.

Erbland, J., Savarino, J., Morin, S., France, J.L., Frey, M.M., King, M.D.: Air-snow transfer of nitrate on the East Antarctic plateau – Part 2: An isotopic model for the interpretation of deep ice-core records. *Atmos. Chem. Phys. Discuss*., 15,6886-6966, doi:10.5194/acpd-15-6887-2015, 2015.

Fisher, J.A., Jacob, D.J., Wang, Q., Bahreini, R., Carouge, C.C., Cubison, M.J., Dibb, J.E., Diehl, T., Jimenez, J.L., Leibensperger, E.M., Meinders, M.B.T., Pye, H.O.T., Quinn, P.K., Sharma, S., van Donkelaar, A., Yantosca, R.M.: Sources, distribution, and acidity of sulfate-ammonium aerosol in the Arctic in winter-spring, *Atmos. Environ*., 45, 7301-7318, 2011.

Frey, M. M., Savarino, J., Morin, S., Erbland, J., and Martins, J. M. F.: Photolysis imprint in the nitrate stable isotope signal in snow and atmosphere of East Antarctica and implications for reactive nitrogen cycling. *Atmos. Chem. Phys*., 9, 8681-8696, 2009.

Frey, M. M., Brough, N., France, J. L., Anderson, P.S., Traulle, O., King, M.D., Jones, A.E., Wolff, E.W., Savarino, J.: The diurnal variability of atmospheric nitrogen oxides (NO and NO_2) above the Antarctic Plateau driven by atmospheric stability and snow emissions. *Atmos. Chem. Phys*., 13, 3045-3062, doi:10.5194/acp-13-3045-2013, 2013.

Freyer, H. D., Kley, D., Voiz-Thomas, A., Kobel, K.: On the interaction of isotopic exchange processes with photochemical reactions in atmospheric oxides of nitrogen. *J. Geophys. Res. Atmos.*, 98(D8), 14791-14796, 1993.

Gallet, J.-C., Domine, F., Arnaud, L., Picard, G., and Savarino, J.: Vertical profiles of the specific surface area and density of the snow at Dome C and on a transect to Dumont D'Urville, Antarctica – albedo calculations and comparison to remote sensing products. The Cryosphere., 5, 631-649, doi: 10.5194/tc-5-631-2011, 2011.

1181 Geng, L., Alexander, B., Cole-Dai, J., Steig, E.J., Savarino, J., Sofen, E.D., Schauer, A.J.:
1182 Nitrogen isotopes in ice core nitrate linked to anthropogenic atmospheric acidity change.
1183 *Proc. Natl. Acad. Sci*., 111, 16, 5808-5812, doi:10.1073/pnas.1319441111, 2014a.
1184
1185 Geng, L., Cole-Dai, J., Alexander, B., Erbland, J., Savarino, J., Schauer, A. J., Steig, E.J.,
1186 Lin, P., Fu, Q., Zatko, M.C.: On the origin of the occasional springtime nitrate
1187 concentration maximum in Greenland. Snow. Atmos. Chem. Phys., 14, 13361-13376,
1188 doi:10.5194/acp-14-13361-2014, 2014b.

1189 Geng, L., Zatko, M.C., Alexander, B., Fudge, T.J., Schauer, A.J., Murray, L.T., Mickley,
1190 L.J.: Effects of post-depositional processing on nitrogen isotopes of nitrate in the
1191 Greenland Ice Sheet Project 2 (GISP2) ice core. *Geophys. Res. Lett*.,
1192 doi:10.1002/2015GL064218, 2015.

1193 Grannas, A. M., Jones, A. E., Dibb, J., Ammann, M., Anastasio, C., Beine, H. J., Bergin,
1194 M., Bottenheim, J., Boxe, C. S., Carver, G., Chen, G., Crawford, J. H., Domine, F., Frey,
1195 M. M., Guzman, M. I., Heard, D. E., Helmig, D., Hoffman, M. R., Honrath, R. E., Huey,
1196 L. G., Hutterli, M., Jacobi, H. W., Klan, P., Lefer, B., McConnell, J., Plane, J., Sander,
1197 R., Savarino, J., Shepson, P. B., Simpson, W. R., Sodeau, J. R., von Glasow, R., Weller,
1198 R., Wolff, E. W., Zhu, T.: An overview of snow photochemistry: evidence, mechanisms
1199 and impacts. *Atmos. Chem. Phys*., 7, 4329-4373, 2007.
1200
1201 Grenfell, T. C.: A Radiative Transfer Model for Sea Ice With Vertical Structure
1202 Variations. *J. Geophys. Res*., 96, 16991-17001, 1991.
1203
1204 Grenfell, T.C., Warren, S.G, Mullen, P.C.: Reflection of solar radiation by the Antarctic
1205 snow surface at ultraviolet, visible, and near-infrared wavelengths. *J. Geophys. Res*., 99,
1206 18669-18684, 1994.
1207
1208 Handorf, D., Foken, T., Kottmeier, C.: The stable atmospheric boundary layer over an
1209 Antarctic ice sheet. *Boundary-Layer Meteorol*, 91, 165-189, 1999.
1210
1211 Hastings, M.G., Steig, E.J., Sigman, D.M.: Seasonal variations in N and O isotopes of
1212 nitrate in snow at Summit, Greenland: Implications for the study of nitrate in snow and
1213 ice cores. *J. Geophys. Res*., 109, D20306, doi:10.1029/2004JD004991, 2004.
1214
1215 Hastings, M.G., Sigman, D.M., Steig, E.J.: Glacial/interglacial changes in the isotopes of
1216 nitrate from the Greenland Ice Sheet Project (GISP2) ice core. *Global Biogeochem.*
1217 *Cycles*, 19:GB4024, doi:10.1029/2005GB002502, 2005.
1218
1219 Heaton, T. H. E., Spiro, B., Robertson, M. C. S.: Potential canopy influences on the
1220 isotopic composition of nitrogen and sulphur in atmospheric deposition. *Oecologia*, 109,
1221 4, 600-607, 1997.
1222
1223 Helmig, D., Boulter, J., David, D., Birks, J. W., Cullen, N.J., Steffen, K., Johnson, B.J.,
1224 Oltmans, S.J.: Ozone and meteorological boundary-layer conditions at Summit,
1225 Greenland, during 3-21 2000. *Atmos. Environ*., 36, 2595-2608, 2002.

Helmig, D., Johnson, B., Oltmans, S.J., Neff, W., Eisele, F., Davis, D.: Elevated ozone in the boundary layer at South Pole. *Atmos. Environ*., 42, 2788-2803, 2008.

Holtslag, A.A.M., Boville, B.: Local versus nonlocal boundary layer diffusion in a global climate mode*l*. *J. Clim*., 6, 1825–1842, 1993.

Honrath, R.E., Lu, Y., Peterson, M.C., Dibb, J.E., Arsenault, M.A., Cullen, N.J., Steffen, K.: Vertical fluxes of NO_x, HONO, and HNO_3 above the snowpack at Summit, Greenland. *Atmos. Environ*., 36, 2629-2640, 2002.

Hudman, R.C., N.E. Moore, R.V. Martin, A.R. Russell, A.K. Mebust, L.C. Valin, and R.C. Cohen, A mechanistic model of global soil nitric oxide emissions: implementation and space based-constraints, *Atmos. Chem. Phys*., 12, 7779-7795, doi:10.5194/acp-12-7779-2012, 2012.

Jarvis, J. C., Hastings, M.G., Steig, E.J., Kunasek, S.A.: Isotopic ratios in gas-phase HNO_3 and snow nitrate at Summit, Greenland. *J. Geophys. Res*., 114, D17301, doi:10.1029/2009JD012134, 2009.

Jin, Z., Charlock, T.P., Yang, P., Xie, Y., Miller, W.: Snow optical properties for different particle shapes with application to snow grain size retrieval and MODIS/CERES radiance comparison over Antarctica. *Remote. Sens. Environ*., 112, 3563-3581, 2008.

Jones, A.E., Anderson, P.S., Wolff, E.W., Turner, J., Rankin, A.M., Colwell, S.R.: A role for newly forming sea ice in springtime polar tropospheric ozone loss? Observational evidence from Halley station, Antarctica. *J. Geophys. Res*., 111, D08306, doi:10.1029/2005JD006566, 2006.

Jones, A.E., Wolff, E.W., Salmon, R.A., Bauguitte, S.J.-B., Roscoe, H.K., Anderson, P.S., Ames, D., Clemitshaw, K.C., Fleming, Z.L., Bloss, W.J., Heard, D.E., Lee, J.D., Read, A.K., Hamer, P., Shallcrossm, D.E., Jackson, A.V., Walker, S.L., Lewis, A.C., Mills, G.P., Plane, J.M.C., Saiz-Lopez, A., Sturges, W.T., Worton, D.R.: Chemistry of the Antarctic Boundary Layer and the Interface with Snow: an overview of the CHABLIS campaign. *Atmos. Chem. Phys*., 8, 3789-3803, 2008.

King, J.C., Argentini, S.A., Anderson, P.S.: Contrasts between the summertime surface energy balance and boundary layer structure at Dome C and Halley stations, Antarctica. *J. Geophys. Res*., 111, D02105, doi:10.1029/2005JD006130, 2006.

Klein, K.: Variability in dry Antarctic firn; Investigations on spatially distributed snow and firn samples from Dronning Maud Land, Antarctica. Ph.D. Thesis, Universitat Bremen. hdl: 10013/epic.44893. http://nbn-resolving.de/urn:nbn:de:gbv:46-00104117-15, date last access: April 15, 2014.

Kodama, Y., Wendler, G., Ishikawa, N.: The diurnal variation of the boundary layer in summer in Adelie Land, Eastern Antarctica. *J. Appl. Met*., 28, 16-24, 1989.

Konig-Langlo, G., King, J., Pettre, P., Climatology of the three coastal Antarctic stations Durmont D'urville, Neumayer, and Halley. *J. Geophys. Res*., D9, 103, 10935-10946, 1998.

Lee, H., Henze, D.K., Alexander, B., Murray, L.T.: Investigating the sensitivity of surface-level nitrate seasonality in Antarctica to primary sources using a global model. *Atmos. Environ*., 89, 757-767, doi:10.1016/j.atmosenv.2014.03.003, 2014.

Legrand, M.R., Kirchner, S.: Origins and variations of nitrate in South Polar precipitation. *J. Geophys. Res*., 95, 3493-3507, 1990.

Levy, H., Moxim, W.J., Klonecki, A.A., Kasibhatla, P.S.: Simulated tropospheric NOx: Its evaluation, global distribution and individual source contributions. *J. Geophys. Res*., 104, 26279-26306, 1999.

Libois, Q., Picard, G., France, J. L., Arnaud, L., Dumont, M., Carmagnola, C. M., King, M. D.: Grain shape influence on light extinction in snow. *The Cyrosphere*, 7, 1803-1818, doi:10.5194/tc-7-1803-2013, 2013.

Lin, J. T., McElroy, M.B.: Impacts of boundary layer mixing on pollutant vertical profiles in the lower troposphere: Implications to satellite remote sensing. *Atmos. Environ*., 44, 1726-1749, doi:10.1016/j.atmosenv.2010.02.009, 2010.

Liu, H., Jacob, D.J., Bey, I., Yantosca, R.M.: Constraints from ^{210}Pb and ^{7}Be on wet deposition and transport in a global three-dimensional chemical tracer model driven by assimilated meteorological fields, *J. Geophys. Res.*, *106*(D11), 12,109-112,128, 2001.

Logan, J.A., Nitrogen oxides in the troposphere: Global and regional budgets. *J. Geophys. Res*., 88(C15), 10785-10807, doi:10.1029/JC088iC15p10785, 1983.

Mack, J., and Bolton, J. R.: Photochemistry of nitrite and nitrate in aqueous solution: A review. *J. Photochem. Photobiol*. A., 128, 1-13, 1999.

Mao, J., Jacob, D.J., Evans, M.J., Olson, J.R., Ren, X., Brune, W.H., St. Clair, J.M., Crounse, J. D., Spencer, K.M., Beaver, M.R., Wennberg, P.O., Cubison, M.J., Jimenez, J.L., Fried, A., Weibring, P., Walega, J.G., Hall, S.R., Weinheimer, A.J., Cohen, R.C., Chen, G., Crawford, J.H., Jaegle, L., Fisher, J.A., Yantosca, R.M., Le Sager, P., Carouge, C.: Chemistry of hydrogen oxide radicals (HO_x) in the Arctic troposphere in spring. *Atmos. Chem. Phys*., 10, 5823-5838, doi:10.5194/acp-10-5823-2010, 2010.

Mayewski, P. A., and Legrand, M. R.: Recent increase in nitrate concentration of Antarctic snow. *Nature,* 346, 258-260, 1990.

Meusinger, C., Berhanu, T.A., Erbland, J., Savarino, J., Johnson, M.S.: Laboratory study of nitrate photolysis in Antarctic snow. I. Observed quantum yield, domain of photolysis, and secondary chemistry. *J. Chem. Phys*., 140, 244305, doi:10.1063/1.4882898, 2014.

Morin, S., Savarino, J., Frey, M.M., Domine, F., Jacobi, H.-W., Kaleschke, L., Martins, J.M.F.: Comprehensive isotopic composition of atmospheric nitrate in the Atlantic Ocean boundary layer from 65°S to 79°N. *J. Geophys. Res*., 114, D05303, doi:10.1029/208JD010696, 2009.

Mulvaney, R., Wagenbach, D., Wolff, E.W.: Postdepositional change in snowpack nitrate from observation of year-round near-surface snow in coastal Antarctica. *J. Geophys. Res*., 103, 11021-11031, 1998.

Murray, L.T., Jacob, D.J., Logan, J.A., Hudman, R.C., Koshak, W.J.: Optimized regional and interannual variability of lightning in a global chemical transport model constrained by LIS/OTD satellite data, *J. Geophys. Res*., 117, D20307, 2012.

Neff, W., Helmig, D., Grachev, A., Davis, D.: A study of boundary layer behaviour associated with high concentrations at the South Pole using a minisoder, tethered balloon, and a sonic anemometer. *Atmos. Environ*., 42, 2762-2779, doi:10.1029/2012JD017934, 2008.

Oliver, J.G.J., Van Aardenne, J.A., Dentener, F.J., Pagliari, V., Ganzeveld, L.N., Peters, J.A.H.W.: Recent trends in global greenhouse gas emissions: regional trends 1970-2000 and spatial distribution of key sources in 2000. Env. Sci., 2(2-3), 81-99, doi:10.1080/15693430500400345, 2005.

Oncley, S., Buhr, M., Lenschow, D., Davis, D., Semmer, S.: Observations of summertime NO fluxes and boundary-layer height at the South Pole during ISCAT 2000 using scalar similarity. *Atmos. Environ*., 38, 5389-5398, doi:10.1016/j.atmosevn.2004.05.053, 2004.

Parish, T. R., and D. H. Bromwich (2007), Reexamination of the near-surface airflow over the Antarctic continent and implications on atmospheric circulations at high southern latitudes, *Monthly Weather Review*, *135*, 1961-1973.

Pratt, K. A., Custard, K. D., Shepson, P. B., Douglas, T. A., Pohler, D., General, S., Zielcke, J., Simpson, W. R., Platt, U., Tanner, D. J., Huey, L. G., Carlsen, M., Stirm, B. H.: Photochemical production of molecular bromine in Arctic surface snowpacks. *Nature*, 6, 351-356, doi:10.1038/NGEO1779, 2013.

Price, C., Rind, D.: A simple lightning parameterization for calculating global lightning distributions. *J. Geophys. Res*., **97**, 9919–9933, 1992.

Rothlisberger, R., Hutterli, M. A., Sommer, S., Wolff, E. W., and Mulvaney, R.: Factors controlling nitrate in ice cores: Evidence from the Dome C deep ice core. J. Geophys. Res., 105, 20565-20572, 2000.

Sander, S. P., Friedl, R.R., Golden, D.M., Kurylo, M.J., Moortgat, G.K., Keller-Rudek, H., Wine, P.J., Ravishankara, A.R., Kolb, C.E., Molina, M.J., Finalyson-Pitts, B.J., Huie, R.E., Orkin, V.L.: Chemical kinetics and photochemical data for use in atmospheric studies evaluation number 15. JPL Publications, Pasadena, 1-523, 06-2, 2006.

Savarino, J., Kaiser, J., Morin, S., Sigman, D.M., Thiemens, M.H.: Nitrogen and oxygen isotopic constraints on the origin of atmospheric nitrate in coastal Antarctica. *Atmos. Chem. Phys*., 7, 1925-1945, 2007.

Shi, G., Buffen, A.M., Hastings, M.G., Li, C., Ma, H., Li, Y., Sun, B., An, C., Jiang, S.: Investigation of post-depositional processing of nitrate in East Antarctica snow: isotopic constraints on photolytic loss, re-oxidation, and source inputs. *Atmos. Chem. Phys.*,15, 9435-9453, doi: 10.5194/acpd-15-9435-2015 2015.

Sjostedt, S.J., Huey, L.G., Tanner, D.J., Peischl, J., Chen, G., Dibb, J.E., Lefer, B., Hutterli, M.A., Beyersdorf, A.J., Blake, N.J., Blake, D.R., Sueper, D., Ryerson, T., Burkhart, J., Stohl, A.: Observations of hydroxul and the sum of peroxy radicals at Summit, Greenland during summer 2003. *Atmos. Environ*., 41, 5122-5137, 2007.

Slusher, D. L., Huey, L. G., Tanner, D. J., Chen, G., Davis, D. D., Buhr, M., Nowak, J. B., Eisele, F. L., Kosciuch, E., Mauldin, R. L., Lefer, B. L., Shetter, R. E., Dibb, J. E.: Measurements of pernitric acid at the South Pole during ISCAT 2000. *Geophys. Res. Lett*., 29, 21, doi:10.1029/2002GL015703, 2002.

Sofen, E.D., Alexander, B., Steig, E.J., Thiemens, M.H., Kunasek, S.A., Amos, H.M., Schauer, A.J., Hastings, M.G., Bautista, J., Jackson, T.L., Vogel, L.E., McConnell, J.R., Pasteris, D.R., Saltzmann, E.S.: WAIS Divide ice core suggests sustained changes in the atmospheric formation pathways of sulfate and nitrate since the 19th century in the extratropical Southern Hemisphere. *Atmos. Chem. Phys*., 14, 5749-5769, doi:10.5194/acp-14-5749-2014, 2014.

Thomas, J. L., Dibb, J. E., Huey, L. G., Liao, J., Tanner, D., Lefer, B., von Glasow, R., Stutz, J.: Modeling chemistry in and above snow at Summit, Greenland – Part 2: Impact of snowpack chemistry on the oxidation capacity of the boundary layer. *Atmos. Chem. Phys*., 12, 6537-6554, doi:10.5194/acp-12-6537-2012, 2012.

Thompson, A.M., The oxidizing capacity of the Earth's atmosphere: Probable past and future changes. *Science*, 256, 1157-1165, 1992.

Travouillon, T., Ashley, M.C.B., Burton, M.G., Storey, J.W.V., Loewenstein, R.F.: Atmospheric turbulence at the South Pole and its implications for astronomy. *Astronom. And Astrophys*., 400, 1163-1172, doi:10.1051/0004-6361:20021814, 2003.

UNEP/WMO. Integrated Assessment of Black Carbon and Tropospheric Ozone: Summary for Decision Makers, UNON/Publishing Services Section/Nairobi, ISO 14001:2004, 2011.

van Donkelaar, A., R. V. Martin, W. R. Leaitch, A.M. Macdonald, T. W. Walker, D. G. Streets, Q. Zhang, E. J. Dunlea, J. L. Jimenez, J. E. Dibb, L. G. Huey, R. Weber, and M. O. Andreae. Analysis of Aircraft and Satellite Measurements from the Intercontinental Chemical Transport Experiment (INTEX-B) to Quantify Long-Range Transport of East Asian Sulfur to Canada. *Atmos. Chem. Phys*., **8**, 2999-3014, 2008.

van der Werf, G.R, Morton, D.C., DeFries, R.S., Giglio, L., Randerson, J.T., Collatz, G.J., Kasibhatla, P.S.: Estimates of fire emissions from an active deforestation region in the southern Amazon based on satellite data and biogeochemical modeling. *Biogeosciences*, **6** (2):235-249, 2009.

Walters, W.W., Goodwin, S.R., Michalski, G.: Nitrogen stable isotope composition $\delta^{15}N$ of vehicle-emitted NO_x. *Environ. Sci. Tech*., 49, 2278-2285, doi:10.1021/es505580v, 2015.

Wang, Y. H., Jacob, D.J., Logan, J.A.: Global simulation of tropospheric O3-NOx hydrocarbon chemistry 1. Model formulation, *J. Geophys. Res.*, *103*, 10,713-710,725, 1998.

Wang, Y., Choi, Y., Zeng, T., Davis, D., Buhr, M., Huey, G. L., and Neff, W.: Assessing the photochemical impact of snow NO_x emissions over Antarctica during ANTCI 2003. *Atmos. Environ*., 41, 3944-3958, doi:10.1016/j.atmosenv.2007.01.056, 2008.

Wang, Q., Jacob, D.J., Fisher, J.A., Mao, J., Leibensperger, E.M., Carouge, C.C., Le Sager, P., Kondo, Y., Jimenez, J. L., Cubison, M. J., Doherty, S.: Sources of carbonaceous aerosols and deposited black carbon in the Arctic in winter-spring: implications for radiative forcing. *Atmos. Chem. Phys*., 11, 12453-12473, doi:10.5194/acp-11-12453-2011, 2011.

Weller, R., Minikin, A., Konig-Langlo, G., Schrems, O., Jones, A.E., Wolff, E.W., Anderson, P.S.: Investigating possible causes of the observed diurnal variability in Antarctica NO_y. *Geophys. Res. Lett*., 26, 18, 2853-2856, 1999.

Wesely, M. L.: Parameterization of surface resistances to gaseous dry deposition in regional-scale numerical-models, *Atmos. Env.*, *23*, 1293-130, 1989.

Wespes, C., Emmons, L., Edwards, D. P., Hannigan, J., Hurtmans, D., Saunois, M., Coheur, P.-F., Clerbaux, C., Coffey, M. T., Batchelor, R. L., Lindenmaier, R., Strong, K., Weinheimer, A. J., Nowak, J. B., Ryerson, T. B., Crounse, J. D., and Wennberg, P. O.: Analysis of ozone and nitric acid in spring and summer Arctic pollution using aircraft, ground-based, satellite observations and MOZART-4 model: source attribution and partitioning, *Atmos. Chem. Phys*., 12, 237-259, doi:10.5194/acp-12-237-2012, 2012.

Wild, O., Q. Zhu, and M. J. Prather (2000), Fast-J: Accurate simulation of in- and below-cloud photolysis in global chemical models, *J. Atm. Chem.*, *37*, 245-282.

Wolff, E.W.: Nitrate in polar ice, in *Ice Core Studies of Global Biogeochem. Cycle*s, NATO ASI Ser., Ser. I, pp. 195-224, edited by R.J. Delmas, Springer, New York, 1995.

Wolff, E.W., Jones, A.E., Bauguitte, S. J.-B., Salmon, R.A.: The interpretation of spikes and trends in concentration of nitrate in polar ice cores, based on evidence from snow and atmospheric measurements. *Atmos. Chem. Phys*., 8, 5627-5634, 2008.

Xu, L., Penner, J.E.: Global simulations of nitrate and ammonium aerosols and their radiative effects. *Atmos. Chem. Phys*., 12, 9479-9504, doi:10.5194/ac[-12-9479-2012, 2012.

Zatko, M.C., Grenfell, T.C., Alexander, B., Doherty, S.J., Thomas, J.L., Yang, X., The influence of snow grain size and impurities on the vertical profiles of actinic flux and associated NO_X emissions on the Antarctic and Greenland ice sheets. *Atmos*. *Chem*. *Phys*., 13, 3547-3567, doi:10.5194/acp-13-3547-2013, 2013.

Zatko, M.C. and Warren, S.G.: East Antarctic sea ice in spring: spectral albedo of snow, nilas, frost flowers, and slush; and light-absorbing impurities in snow. *Ann. Glaciol. Special Issue: Sea ice in a changing environment,* 56(69), 53-64, doi:10.3189/2015AoG69A574, 2015.

Zhang, L., S. Gong, J. Padro, and L. Barrie.: A size-segregated particle dry deposition scheme for an atmospheric aerosol module, *Atmos. Env.*, *35*, 549-560, 2001.

Zhu, C., Xiang, B., Chu, L.T., Zhu, L.: 308 nm Photolysis of Nitric Acid in the Gas Phase, on Aluminum Surfaces, and on Ice Films. *J. Phys. Chem. A*., 114, 2561-2568, doi: 10.1021/jp909867a, 2010.

1498 Table 1. Glossary of variables used in this paper.

Variable	Unit	Description
λ	nm	Wavelength
ϕ	molec photon^{-1}	Quantum yield for NO_3^- photolysis
σ_{NO3^-}	cm^2	Absorption cross-section for NO_3^- photolysis
I	photons cm^{-2} s^{-1} nm^{-1}	Actinic flux of UV radiation
z_e	cm	e-folding depth of UV actinic flux in snow
z_{3e}	cm	Depth of snow photic zone
α_r	kg m^{-2} yr^{-1}	Total annual snow accumulation rate
C_{BC}	ng g^{-1}	Annual mean snow black carbon concentration
r_e	μm	Radiation equivalent mean ice grain radii
ρ_{snow}	kg m^{-3}	Snow density
$Kext_{tot}$	cm^{-1}	Bulk extinction coefficient for snow
$[NO_3^-]_{top}$	ng g^{-1}	Mean NO_3^- concentration in top 2 cm of snow
$[NO_3^-]_{bot}$	ng g^{-1}	Mean NO_3^- concentration from 2-cm depth to the bottom of the snow photic zone
EF	unitless	NO_3^- enhancement factor in top 2 cm of snow
F_p	fraction	Fraction of photolabile NO_3^- in snow
$[NO_3^-]_{bot}$ x F_p	ng g^{-1}	Mean NO_3^- concentration from 2-cm depth to the bottom of the snow photic zone scaled by fraction of photolabile NO_3^- in snow
ε	‰	Fractionation constant for NO_3^- photolysis
$\overline{F_{NOx}}$	molec cm^{-2} s^{-1}	Mean summer flux of snow-sourced NO_x
F_{NOx}	ng N m^{-2} yr^{-1}	Annual sum of snow-sourced NO_x flux
F_{PRI}	ng N m^{-2} yr^{-1}	Annual sum of primary NO_3^- deposited to snow
F_R	ng N m^{-2} yr^{-1}	Annual sum of recycled NO_3^- to snow
NRF	unitless	Metric to assess degree of nitrogen recycling in 1 year
$\tau_{NO_3^-_{burial}}$	years/months	Lifetime of NO_3^- against burial below snow photic zone
$\tau_{NO_3^-_{photolysis}}$	months	Lifetime of NO_3^- against photolysis in snow photic zone
$F_{p_{photo}}$	unitless	Fraction of photolabile NO_3^- photolyzed rather than buried below the snow photic zone
f	fraction	Fraction of photolysis-driven loss of NO_3^- from snow
$\delta^{15}N(NO_3^-)$	‰	Nitrogen isotopic composition of NO_3^-

1499
1500
1501
1502
1503
1504
1505
1506
1507
1508
1509
1510

Table 2. Value(s) of parameters used in the model.

Variable	Value(s) used in model	References
ϕ	0.0015-0.0052 molec photon^{-1}[a] (Antarctica) 0.0032-0.0069 molec photon^{-1}[a] (Greenland)	Chu and Anastasio [2003]
σ_{NO3^-}	2.7×10^{-20} cm^2 (λ=298-307 nm) 2.4×10^{-20} cm^2 (λ=307-312 nm) 1.9×10^{-20} cm^2 (λ=312-320 nm) 2.3×10^{-21} cm^2 (λ=320-345 nm)	Sander et al. [2006]
ε	-47.9‰	Berhanu et al. [2014]
r_e	86.0-235.0 μm[b] (Antarctica) 73.0-211.0 μm[b] (Greenland)	Carmagnola et al. [2013] Gallet et al. [2011]
ρ_{snow}	260-360 kg m^{-3}[b] 235-350 kg m^{-3}[b]	Gallet et al. [2011] Carmagnola et al. [2013]
EF	6[c] (Antarctica) 1[c] (Greenland)	Dibb et al. [2004, 2007] Erbland et al. [2013] Frey et al. [2009] Mayewski and Legrand [1990] Rothlisberger et al. [2000]
$[NO_3^-]_{bot}$	60 ng g^{-1}[d] 132 ng g^{-1}[e]	Bertler et al. [2005] Burkhart et al. [2009] Dibb et al. [2007] Honrath et al. [2002] Geng et al. [2014b]

[a]Temperature-dependent equation from Chu and Anastasio [2003] used. The modeled temperatures ranged from 237-271K across Antarctica and 257-280K across Greenland.

[b]Vertical profiles of r_e range from 86 μm at the snow surface to 332 μm at 300-cm depth in Antarctica and from 73 μm at the snow surface to 211 μm at 300-cm depth in Greenland and are not varied spatially or temporally. Vertical profiles of ρ_{snow} range from 260 kg m^{-3} at the snow surface to 360 kg m^{-3} at 300-cm depth in Antarctica and from 235 kg m^{-3} at the snow surface to 350 kg m^{-3} at 300-cm depth in Greenland and are not varied spatially or temporally. Observations from Gallet et al. [2011] (Dome C) are used across Antarctica and from Carmagnola et al. [2013] (Summit) are used across Greenland. The deepest observed r_e and ρ_{snow} values are used for all modeled r_e and ρ_{snow} values at deeper snow depths.

[c]Median of observed NO_3^- enhancement factors in Antarctica (1-17) and low end of observed NO_3^- enhancement factors in Greenland (1-2).

[d]Median of observed sub-surface snow NO_3^- mixing ratios from the ITASE campaign [*Bertler et al*., 2005].

[e]Average NO_3^- concentrations from buried snow layer presented in Table 3 are used.

Table 3. Dependence of mean austral summer (DJF) flux of snow-sourced NO_x ($\overline{F_{NOx}}$) in Antarctica on quantum yield (ϕ), the fraction of photolabile NO_3^- (F_p), snow NO_3^- concentrations below 2 cm ($[NO_3^-]_{bot}$), the radiation equivalent ice grain radius (r_e), the bulk snow extinction coefficient ($Kext_{tot}$), the NO_3^- concentration enhancement factor in the top 2 cm (EF), and snow black carbon concentration.

Parameter	Base case values (where $\overline{F_{NOx}}$ = 0.5-7.8x10^8 molec cm^{-2} s^{-1})	Values used in sensitivity studies	$\overline{F_{NOx}}$ range in sensitivity studies (x10^8 molec cm^{-2} s^{-1}) (Factor changes compared to $\overline{F_{NOx}}$ in base case, unitless)
Quantum yield (ϕ)	0.002 molec $photon^{-1}$ [a]	0.6 molec $photon^{-1}$	5-2600 (10.0-333.0)
Fraction of photolabile NO_3^- (F_p)	0.01-0.99 (spatial variation, Figure 3c)	Set to 1 everywhere	3.7-9.6 (1.2-7.4)
Sub-surface snow NO_3^- ($[NO_3^-]_{bot}$)	60.0 ng g^{-1} [b]	30-120 ng g^{-1}	0.3-15.8 (0.6-2.0)
Radiation equivalent mean ice grain radii (r_e)	Jan: 332.0 μm[c] Dec-Feb: 198-332.0 μm[c] Mar-Nov: 86.0-332.0 μm[c]	Study 1: 332.0 μm[d] Study 2: 198-332.0 μm[d] Study 3: 86.0-332.0 μm[d]	0.5-10.2 (1.0-1.3)
Bulk snow extinction coefficient ($Kext_{tot}$)	1.7-6.9x10^3 m^{-1} (spatial variation)	± 20% with respect to base case values	0.5-9.4 (1.0-1.2)
NO_3^- enhancement factor in top 2 cm (EF)	6.0[e]	1-10	0.5-9.3 (1.0-1.2)
Snow black carbon (C_{BC})	0.08-0.6 ng g^{-1} (spatial variation, Figure 3b)	± factor of 2 with respect to base case values	0.5-8.6 (1.0-1.1)

[a] from Chu and Anastasio [2003] at T=244K

[b] median of ITASE campaign [*Bertler et al*., 2005]

[c] r_e is varied vertically and temporally, but uniformly across Antarctica based on Gallet et al. [2011] and Klein [2014]. In January, r_e is constant with depth (332 μm), in December and February, r_e ranges from 198 μm at the snow surface to 332 μm at 300 cm depth, and from March to November, r_e ranges from 86 μm at the surface to 360 μm at 300 cm depth.

[d] in r_e sensitivity study 1, the base-case 'January' r_e profile is applied for every month. In r_e sensitivity study 2, the base-case 'December and February' r_e profile is applied for every month. In r_e sensitivity study 3, the base-case 'March-November' r_e profile is applied for every month.

[e] median of observed EF [*Dibb et al*., 2004, *Frey et al*., 2009, *Mayewski and Legrand*, 1990, *Rothlisberger et al*., 2000].

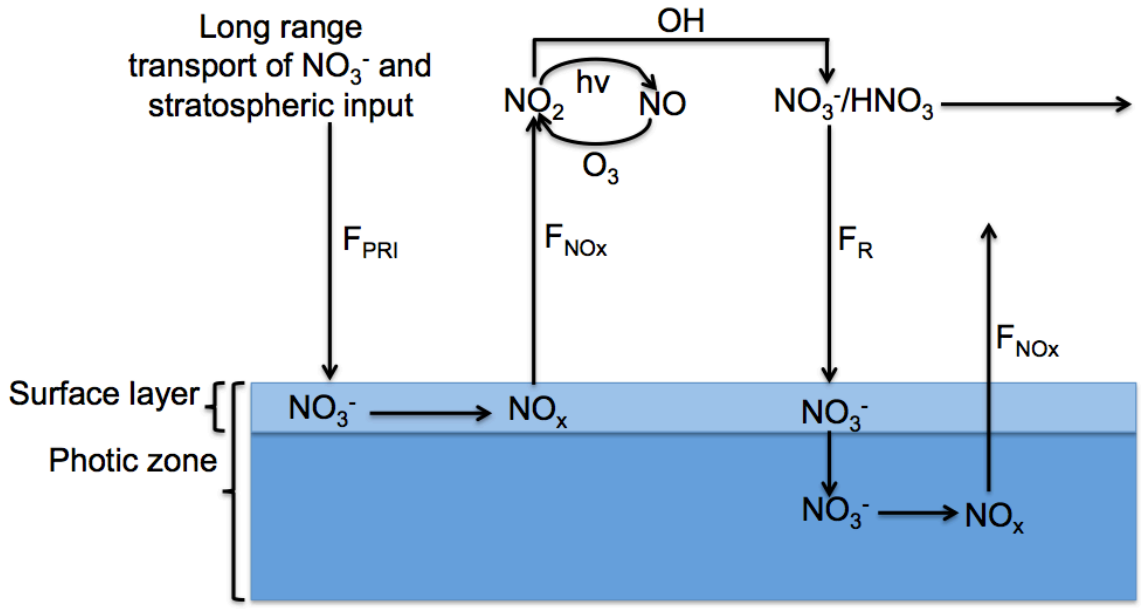

Figure 1. Schematic showing the nitrogen recycling associated with NO_3^- photolysis as included in the model. F_{PRI} (ng N m^{-2} yr^{-1}) is the downward, primary flux of NO_3^- to Antarctica and Greenland originating from long-range transport and the stratosphere, F_{NOx} (ng N m^{-2} yr^{-1}) is the upward flux of snow-sourced NO_x to the boundary layer, and F_R (ng N m^{-2} yr^{-1}) is downward, recycled flux of HNO_3 to the snow surface. The surface snow layer (top 2 cm) is distinguished from the rest of the photic zone because 30-65% of snow-sourced NO_x is produced in the top 2 cm of snowpack [*Zatko et al.*, 2013], and because both NO_3^- concentrations and actinic flux are much higher in the top surface layer compared to deeper layers.

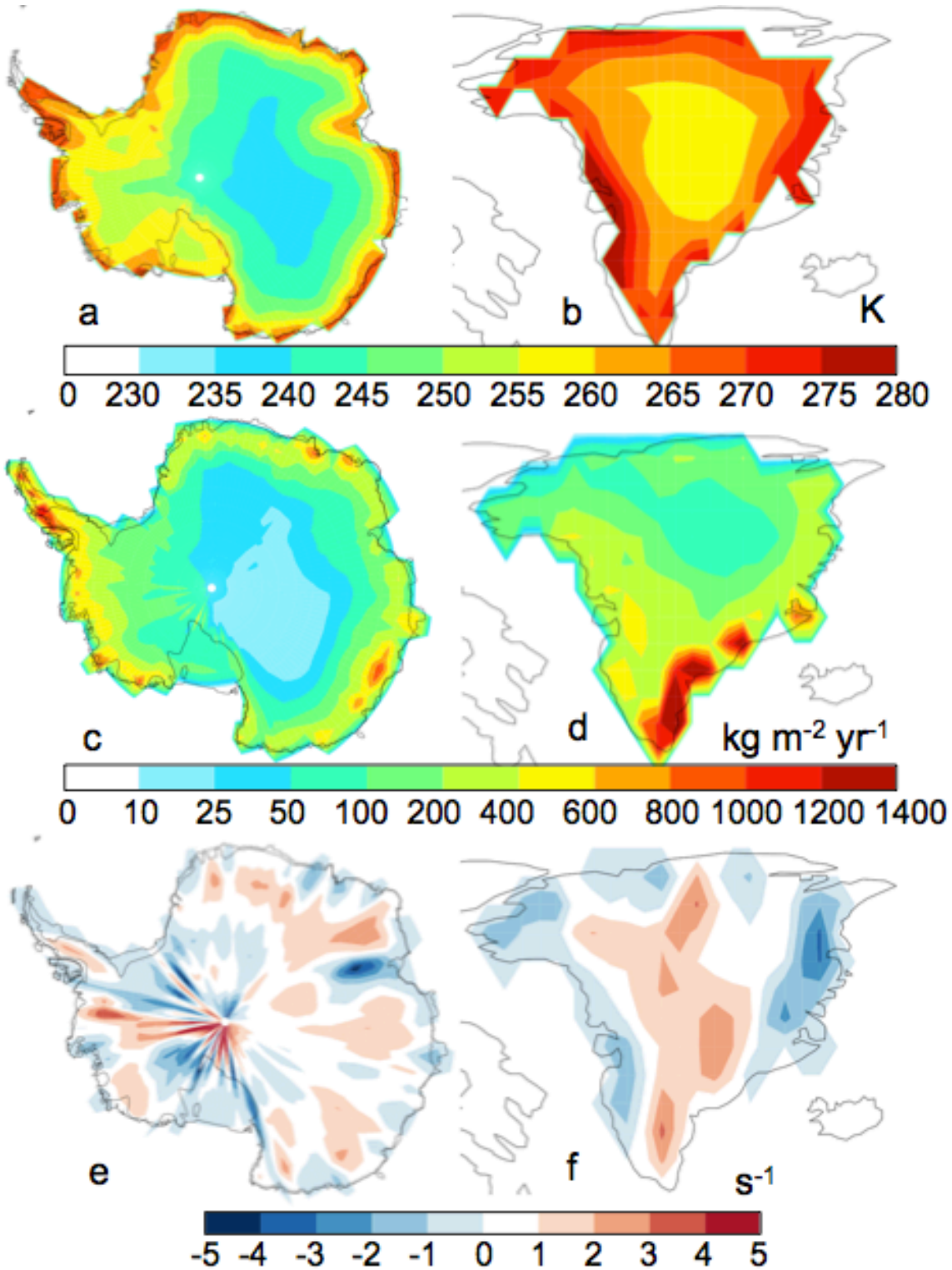

Figure 2. Modeled meteorological variables in GEOS-Chem. (a,b) Mean summer (DJF, Antarctica; JJA, Greenland) air temperature in lowest vertical grid box. (c,d) Annual total snow accumulation rate (kg m^{-2} yr^{-1}) from May 2009 to May 2010. (e,f) Annual mean surface wind divergence (s^{-1}) from May 2009 to May 2010.Blue regions indicate regions of convergence.

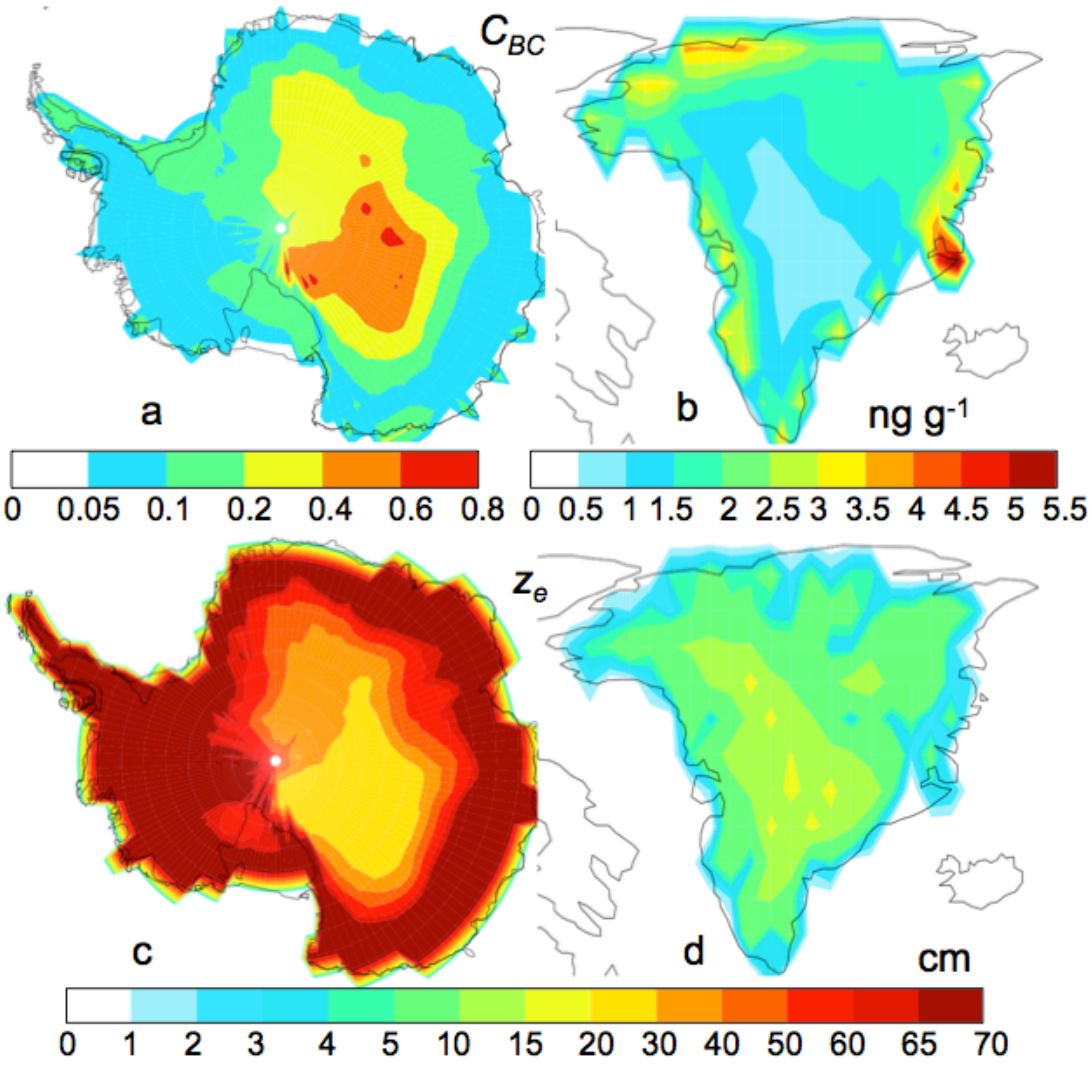

Figure 3. (a,b) Modeled annual mean snow black carbon concentrations (C_{BC}). (c,d) Calculated mean summer (DJF, Antarctica; JJA, Greenland) UV e-folding depth (z_e).

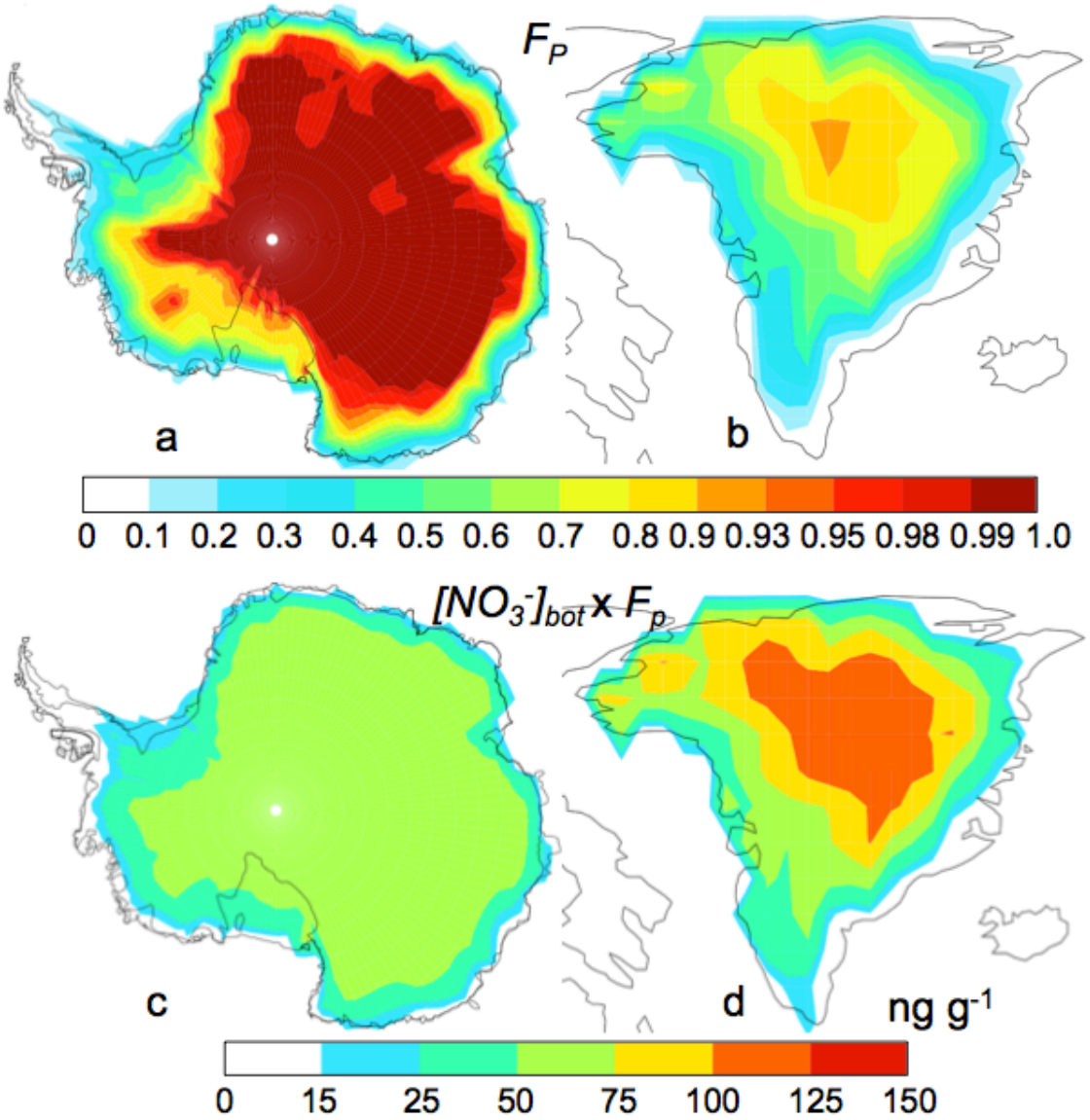

Figure 4. (a,b) Ratio of annual dry-deposited NO_3^- to annual total deposited nitrate, F_P. (c,d) Annual sub-surface snow NO_3^- concentrations ($[NO_3^-]_{bot}$ x F_p) used in the model.

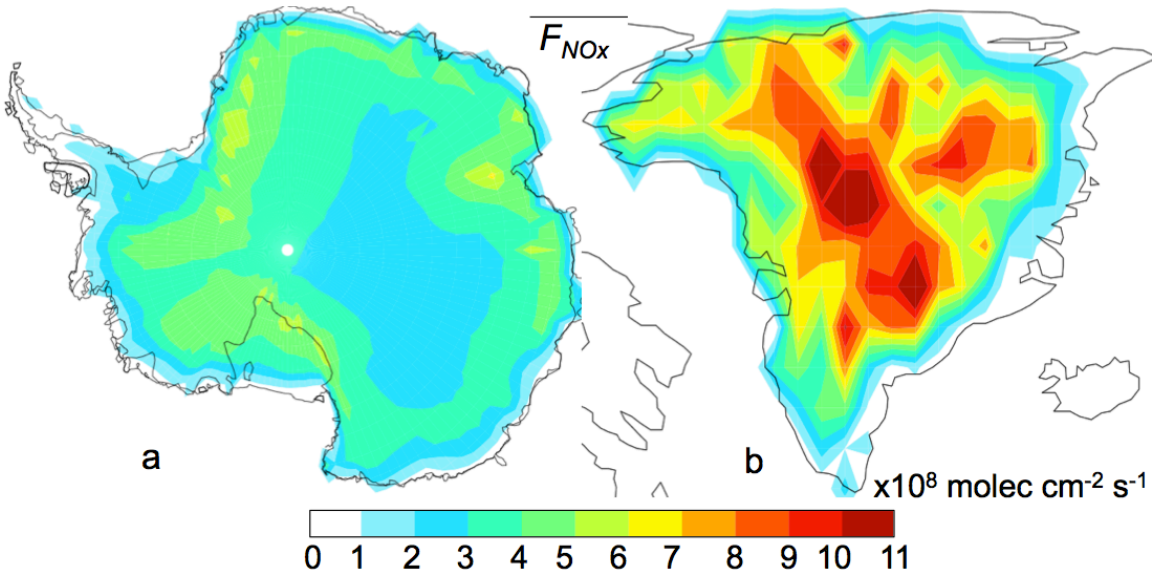

Figure 5. Mean summer (DJF, Antarctica; JJA, Greenland) flux of snow-sourced NO_x from the snow ($\overline{F_{NOx}}$).

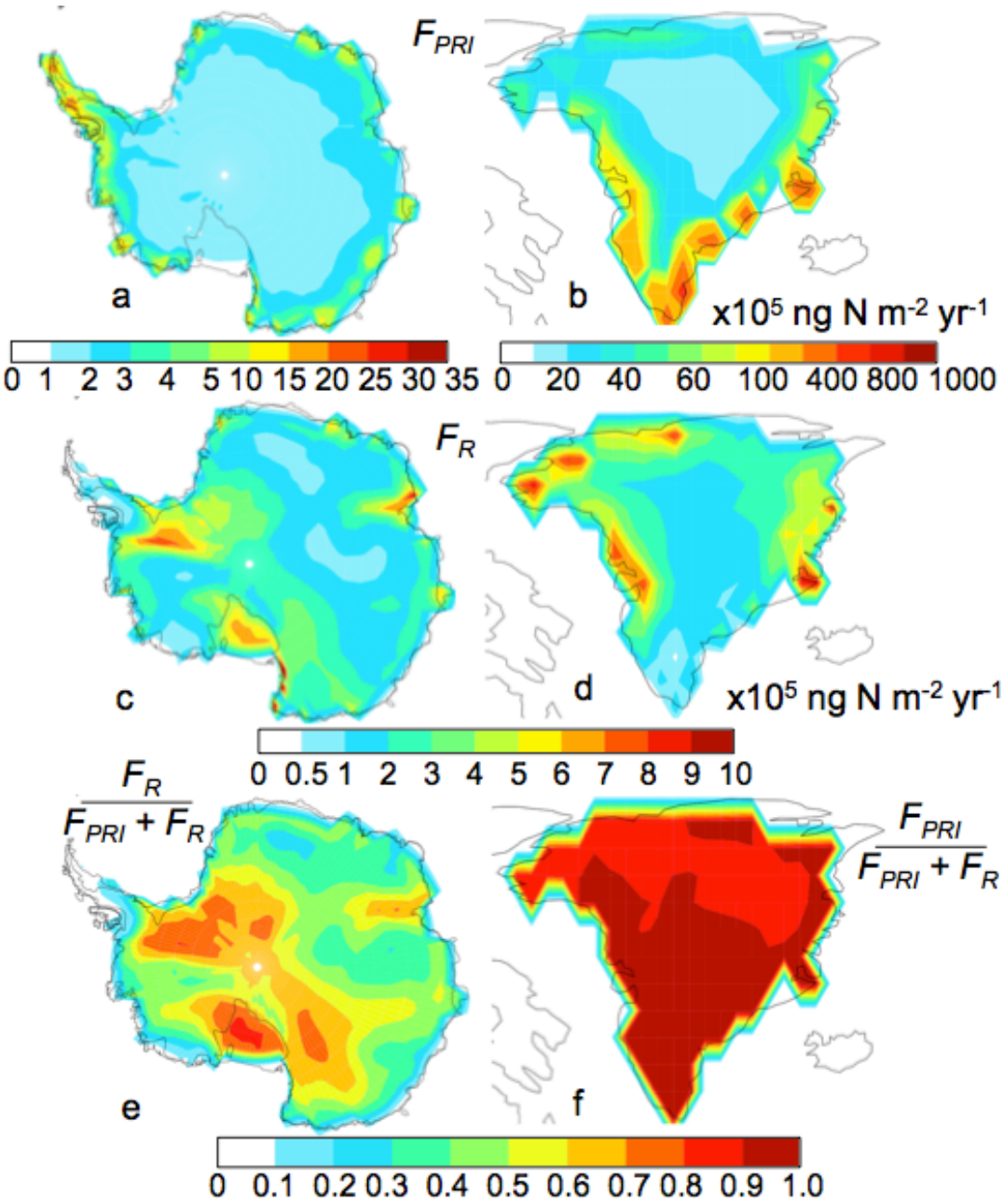

Figure 6. (a,b) Annual wet plus dry deposition flux of primary NO_3^- to the snow (F_{PRI}). (c,d) Annual wet plus dry deposition flux of recycled NO_3^- to the snow (F_R). (e) Ratio of F_R to the total downward NO_3^- flux ($\frac{F_R}{F_{PRI}+F_R}$) for the base case scenario. (f) Ratio of F_{PRI} to the total downward NO_3^- flux ($\frac{F_{PRI}}{F_{PRI}+F_R}$).

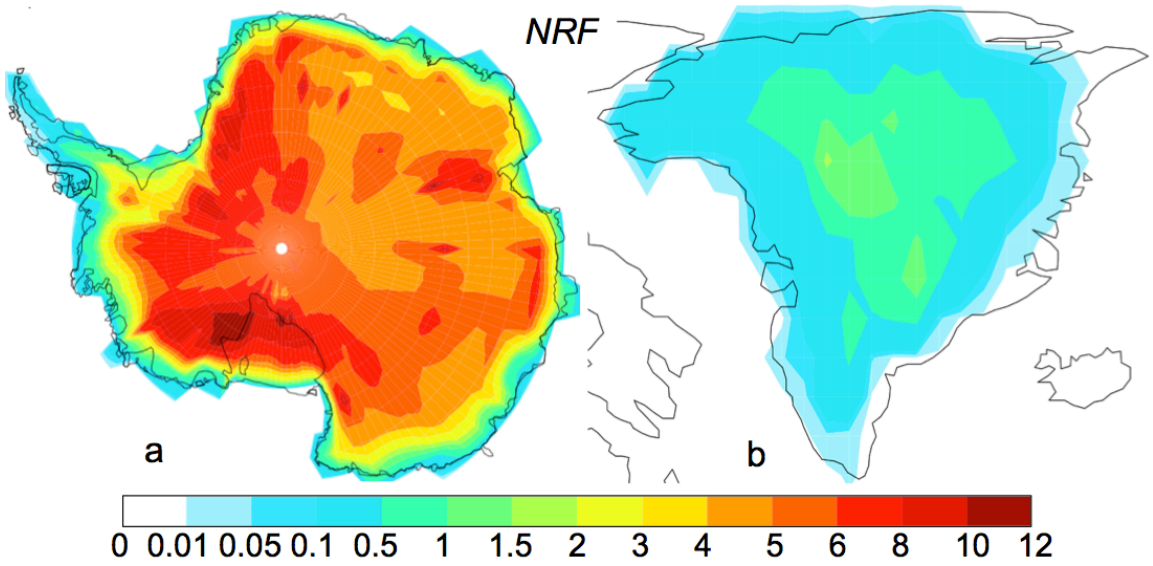

Figure 7. Nitrogen recycling factor (*NRF*, E9).

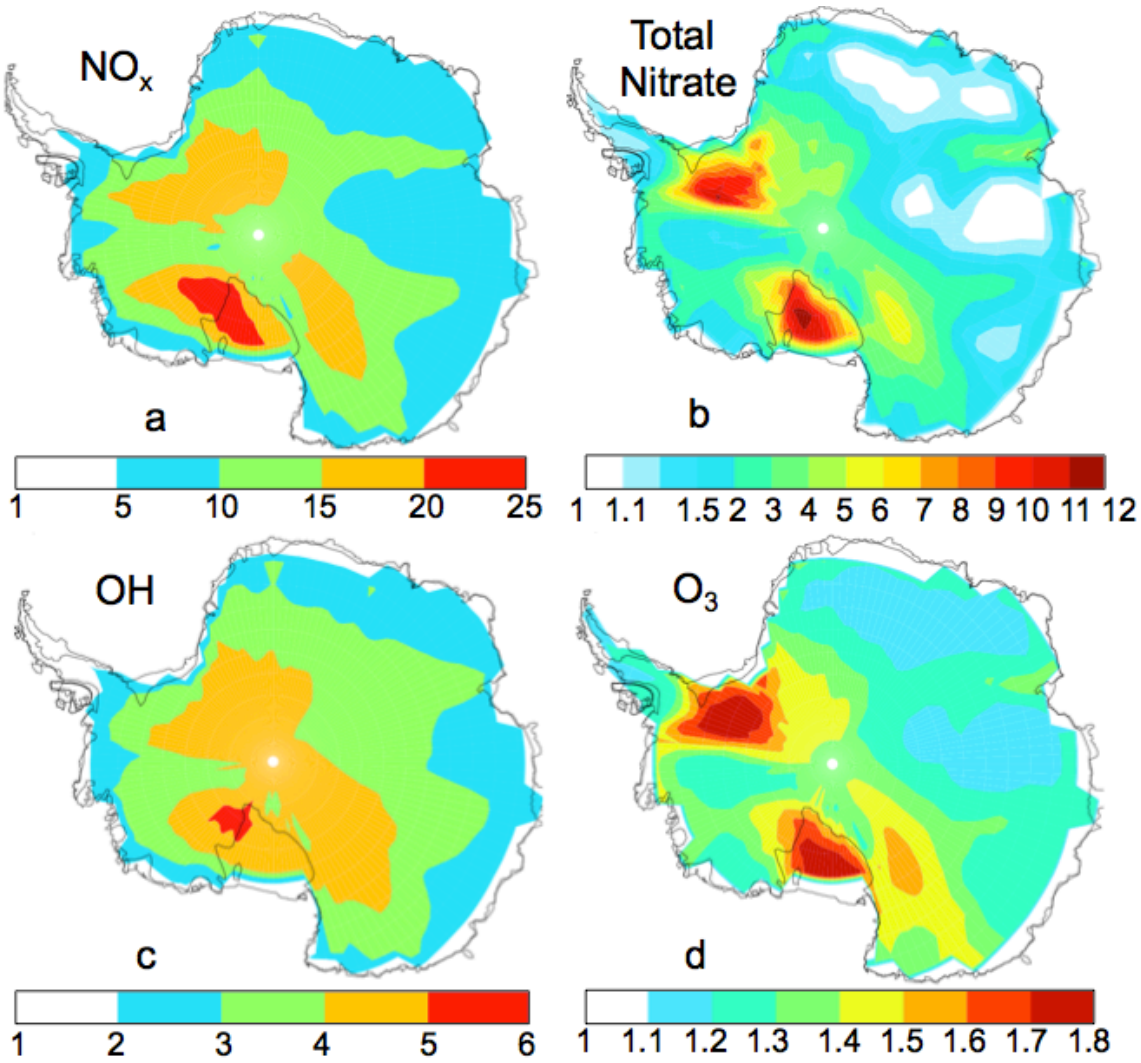

Figure 8. Factor increase in mean austral summer (DJF) boundary layer (a) NO_x, (b) gas+aerosol phase NO_3^-, (c) OH, and (d) O_3 mixing ratios between model runs with F_{NOx} compared to without F_{NOx}.

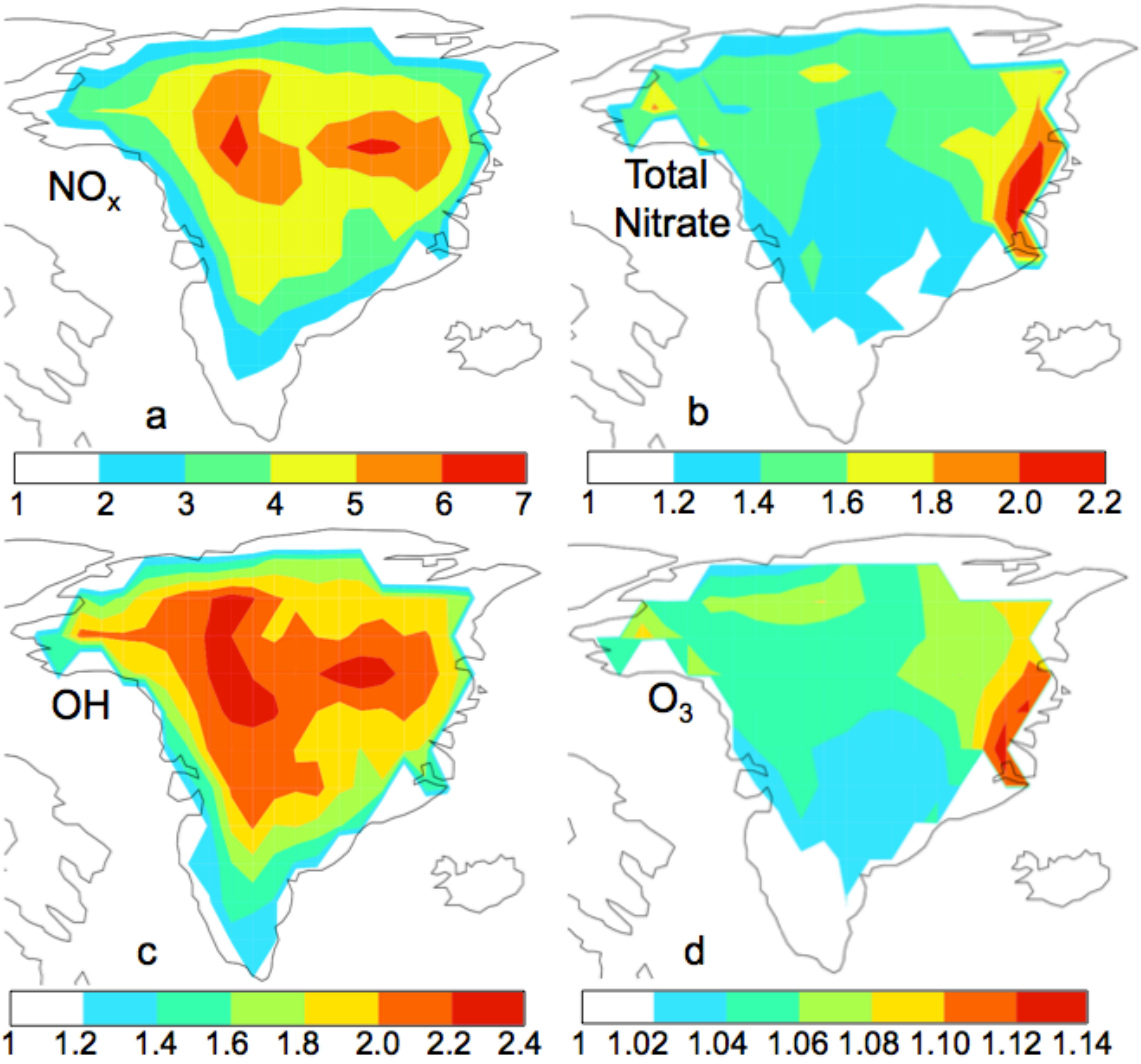

Figure 9. Factor increase in mean summer (JJA) boundary layer (a) NO_x, (b) gas+aerosol phase nitrate, (c) OH, and (d) O_3 mixing ratios between model runs with F_{NOx} compared to without F_{NOx}.

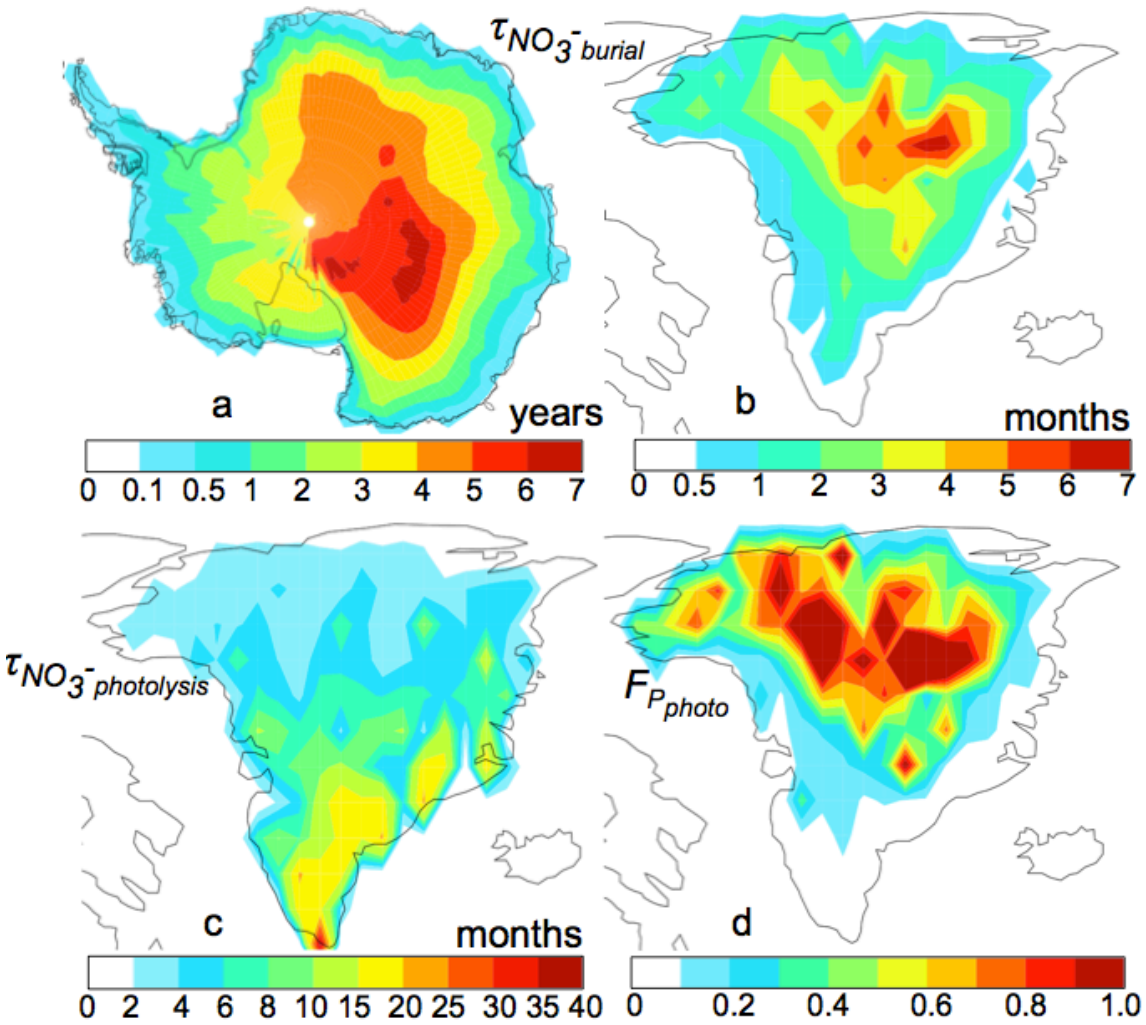

Figure 10. (a,b) Minimum lifetime of NO_3^- against burial below snow photic zone ($\tau_{NO_3^-\,burial}$, E11). (c) Average lifetime of NO_3^- against photolysis in the photic zone in Greenland ($\tau_{NO_3^-\,photolysis}$, E13). (d) Ratio of $\tau_{NO_3^-\,burial}$ to $\tau_{NO_3^-\,photolysis}$ in Greenland ($F_{p_{photo}}$, E12).

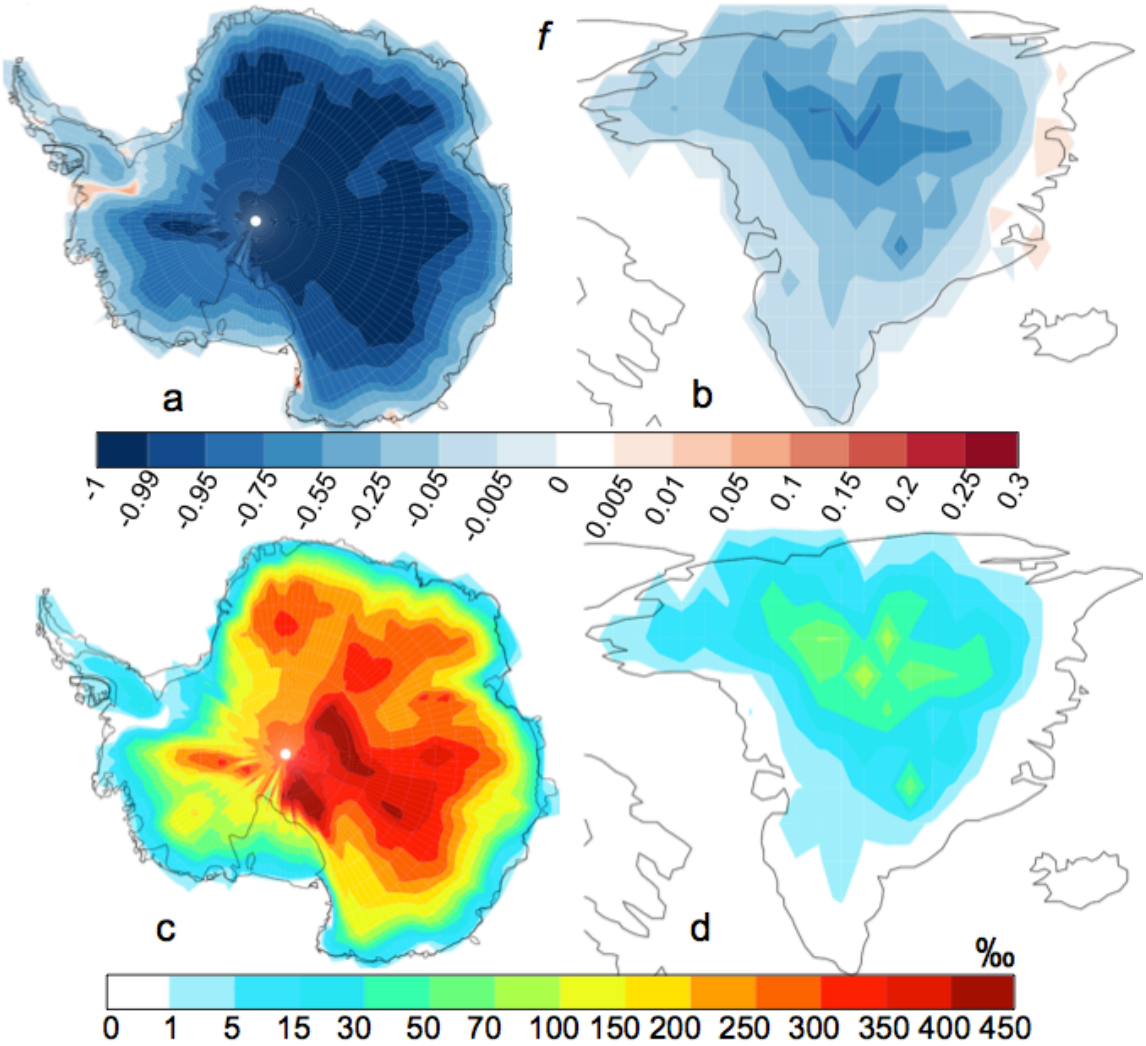

Figure 11. (a,b) Fraction of NO_3^- gained (positive values) or lost (negative values) from the snow through photolysis (*f*, E10). (c,d) Modeled enrichment in ice-core $\delta^{15}N(NO_3^-)$ (E14) due to photolysis-driven loss of NO_3^- in snow. Note the varied color bar scale in Figures 11a and 11b.

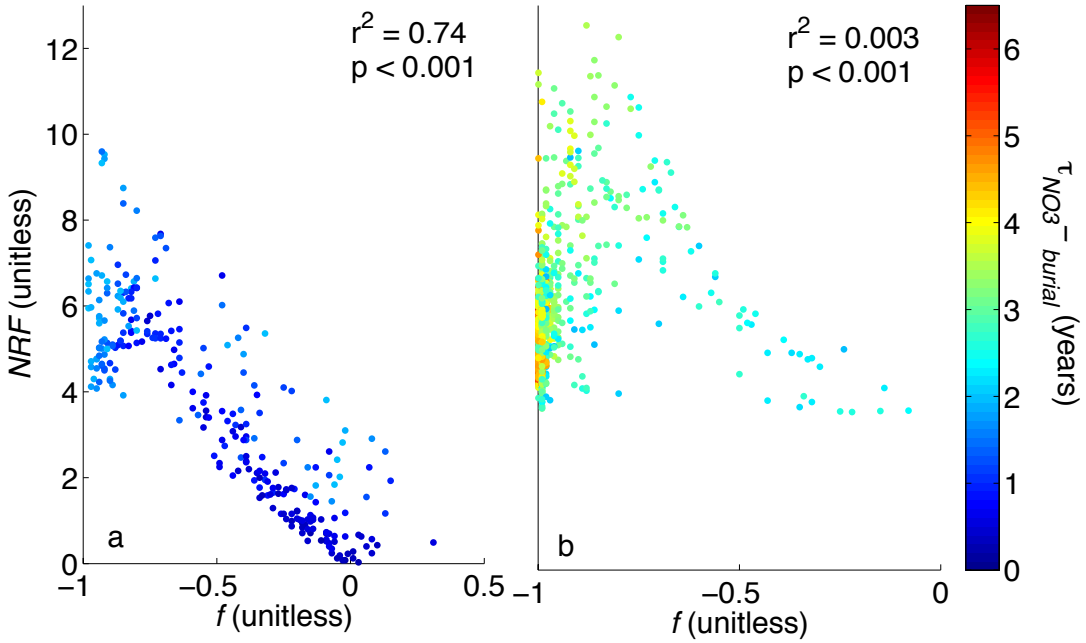

Figure 12. *NRF* versus *f* values across Antarctica. (a) Regions where NO_3^- remains in the photic zone for 2 years or less. (b) Regions where NO_3^- remains in the photic zone for more than 2 years. The color scale represents the number of years NO_3^- remains in the photic zone ($\tau_{NO_3^-\,burial}$).

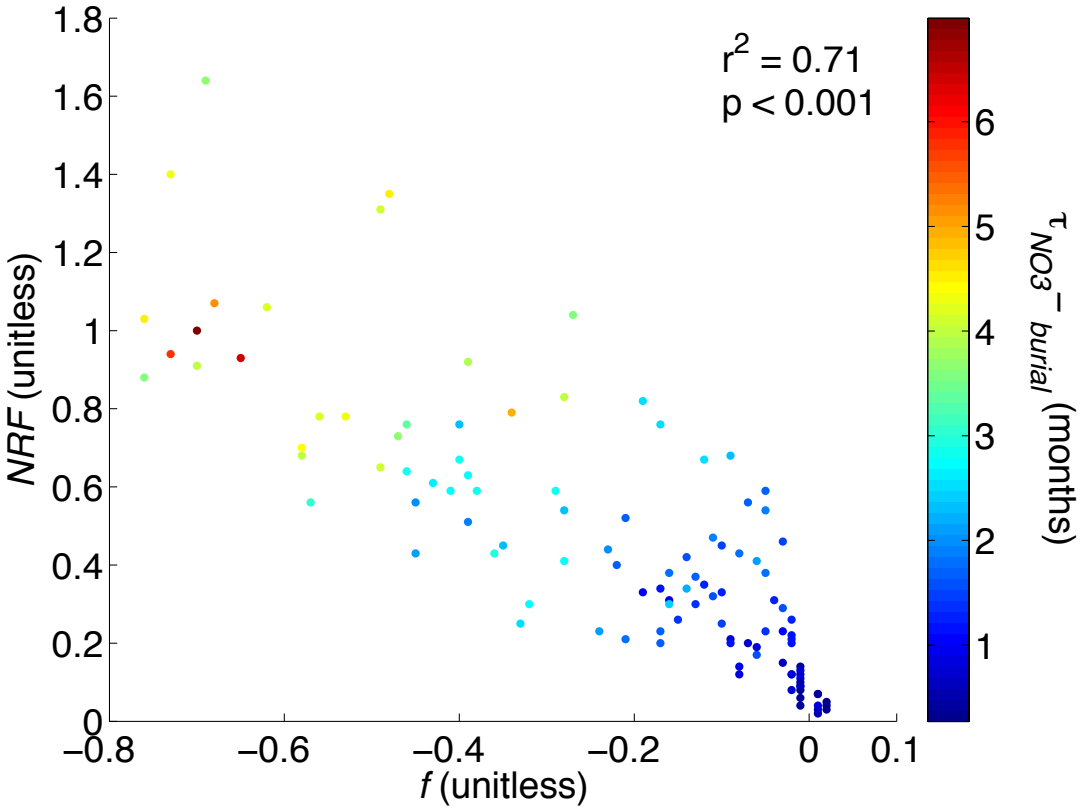

Figure 13. *NRF* versus *f* values across Greenland. The color scale represents the minimum number of months that NO_3^- remains in the photic zone ($\tau_{NO_3^-\,burial}$).

1711 Supplemental Material
1712

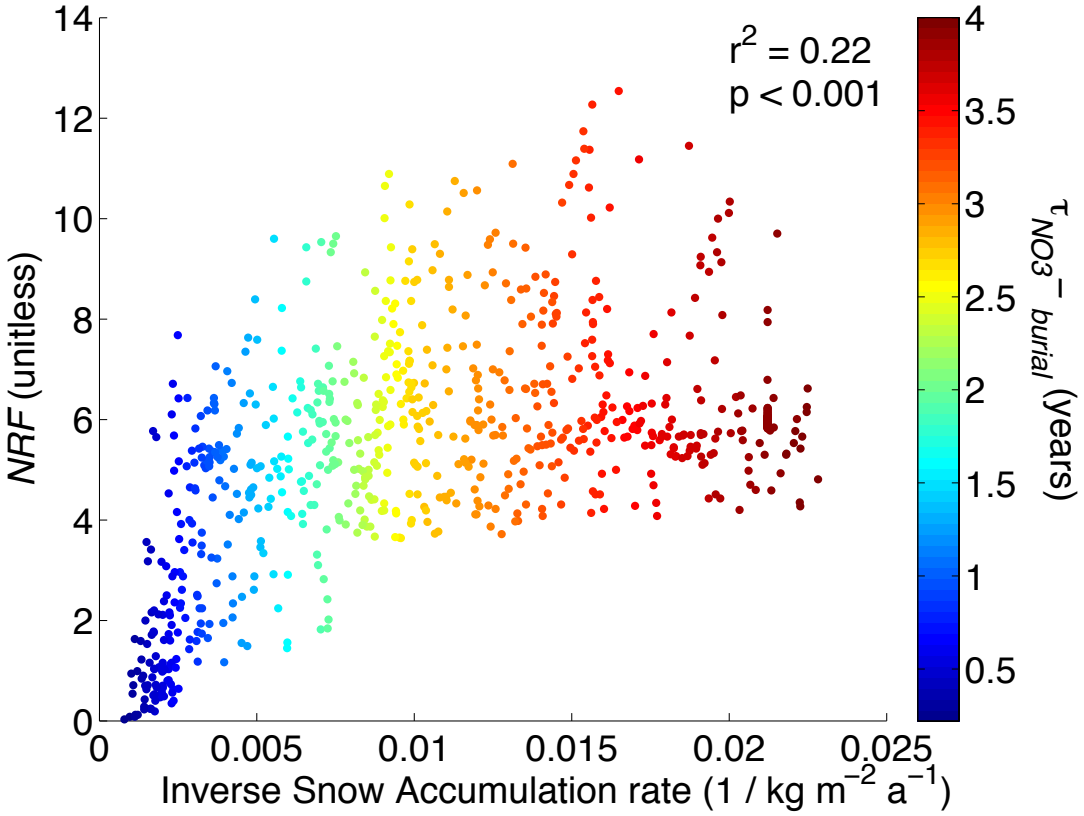

1713
1714 Figure S1. *NRF* versus inverse snow accumulation rate values across Antarctica. The
1715 color scale represents the minimum number of years that NO_3^- remains in the photic zone
1716 ($\tau_{NO_3^-\ burial}$).
1717
1718

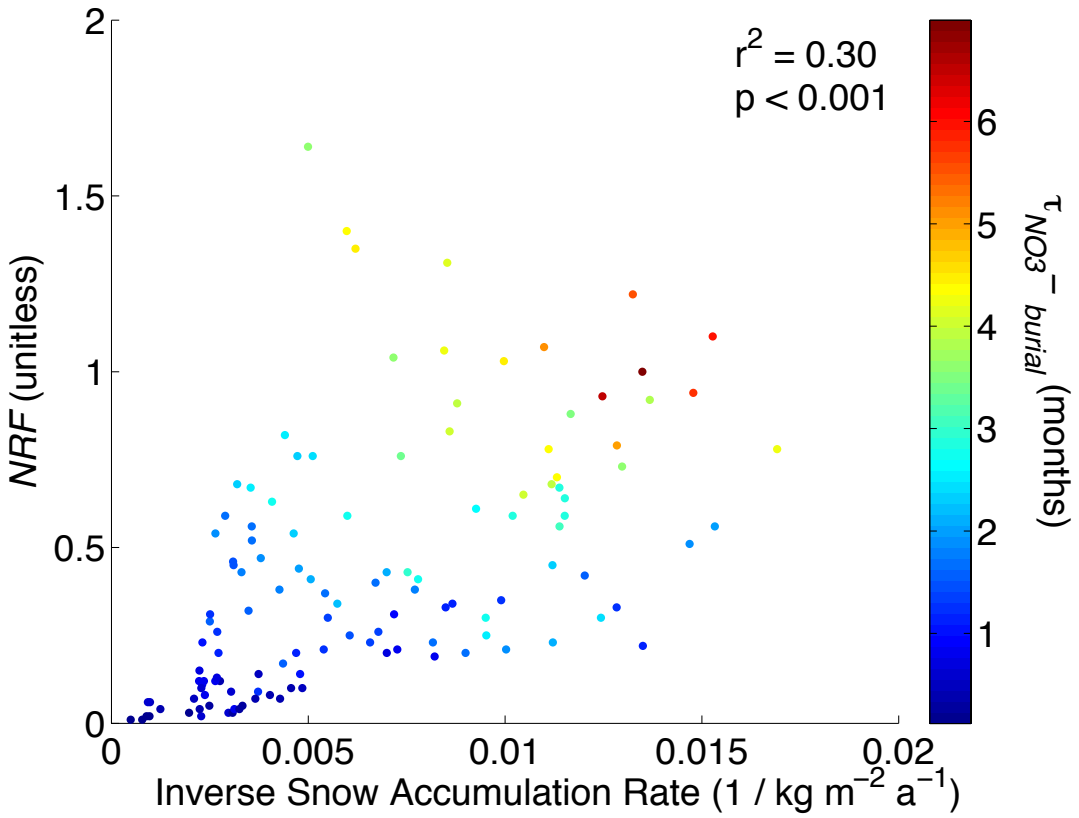

Figure S2. *NRF* versus inverse snow accumulation rate values across Greenland. The color scale represents the minimum number of months that NO_3^- remains in the photic zone ($\tau_{NO_3^-\,burial}$).